

# An Empirical-Bayes Approach to Recovering Linearly Constrained Non-Negative Sparse Signals

Jeremy Vila and Philip Schniter\*

**Abstract**—We propose two novel approaches to the recovery of an (approximately) sparse signal from noisy linear measurements in the case that the signal is a priori known to be non-negative and obey given linear equality constraints, such as simplex signals. This problem arises in, e.g., hyperspectral imaging, portfolio optimization, density estimation, and certain cases of compressive imaging. Our first approach is based on the max-sum version of the generalized approximate message passing (GAMP) algorithm, where we consider several choices of noise prior and sparsity-inducing signal priors, and propose a novel approach to learning the underlying statistical parameters based on the expectation maximization (EM) algorithm. The second is based on the sum-product version of the GAMP algorithm, where we propose the use of a Bernoulli non-negative Gaussian-mixture signal prior and a Laplacian likelihood, and propose an EM-based approach to learning the underlying statistical parameters. In both approaches, the linear equality constraints are enforced by augmenting GAMP’s generalized-linear observation model with noiseless pseudo-measurements. Extensive numerical experiments demonstrate the state-of-the-art performance of our proposed approaches.

## I. INTRODUCTION

We consider the recovery of an (approximately) sparse signal  $\mathbf{x} \in \mathbb{R}^N$  from the noisy linear measurements

$$\mathbf{y} = \mathbf{A}\mathbf{x} + \mathbf{w} \in \mathbb{R}^M, \quad (1)$$

where  $\mathbf{A}$  is a known sensing matrix,  $\mathbf{w}$  is noise, and  $M$  may be  $\ll N$ . In this paper, we focus on non-negative (NN) signals (i.e.,  $x_n \geq 0 \forall n$ ) that obey known linear equality constraints  $\mathbf{B}\mathbf{x} = \mathbf{c} \in \mathbb{R}^P$ . A notable example is *simplex*-constrained signals, i.e.,  $\mathbf{x} \in \Delta^+ \triangleq \{\mathbf{x} \in \mathbb{R}^N : x_n \geq 0 \forall n, \mathbf{1}^\top \mathbf{x} = 1\}$ , occurring in hyperspectral image unmixing [2], portfolio optimization [3], [4], density estimation [5], [6], and other applications. We also consider the recovery of NN sparse signals without the linear constraint  $\mathbf{B}\mathbf{x} = \mathbf{c}$  [7]–[9], which arises in imaging applications [10] and elsewhere [11].

One approach to recovering linearly constrained NN sparse  $\mathbf{x}$  is to solve the  $\ell_1$ -penalized constrained NN least-squares (LS) problem (2) (see, e.g., [4]) for some  $\lambda \geq 0$ :

$$\hat{\mathbf{x}} = \arg \min_{\mathbf{x} \geq 0} \frac{1}{2} \|\mathbf{y} - \mathbf{A}\mathbf{x}\|_2^2 + \lambda \|\mathbf{x}\|_1 \quad \text{s.t.} \quad \mathbf{B}\mathbf{x} = \mathbf{c}. \quad (2)$$

The authors are with the Department of Electrical and Computer Engineering, The Ohio State University, Columbus, OH.

\*Please direct all correspondence to Prof. Philip Schniter, Dept. ECE, The Ohio State University, 2015 Neil Ave., Columbus OH 43210, e-mail: schniter@ece.osu.edu, phone 614.247.6488, fax 614.292.7596.

This work has been supported in part by NSF grants IIP-0968910, CCF-1018368, CCF-1218754, and by DARPA/ONR grant N66001-10-1-4090.

Portions of this work were presented at the 2013 IEEE Internat. Workshop on Computational Advances in Multi-Sensor Adaptive Processing [1].

Although this problem is convex [12], finding a solution can be computationally challenging in the high-dimensional regime. Also, while a larger  $\lambda$  is known to promote more sparsity in  $\hat{\mathbf{x}}$ , determining the best choice of  $\lambda$  can be difficult in practice. For example, methods based on cross-validation, the L-curve, or Stein’s unbiased risk estimator can be used (see [13] for discussions of each), but they require much more computation than solving (2) for a fixed  $\lambda$ . For this reason, (2) is often considered under the special case  $\lambda=0$  [14], where it reduces to linearly constrained NN-LS.

For the recovery of  $K$ -sparse simplex-constrained signals, a special case of the general problem under consideration, the Greedy Selector and Simplex Projector (GSSP) was proposed in [6]. GSSP, an instance of projected gradient descent, iterates

$$\hat{\mathbf{x}}^{i+1} = \mathcal{P}_K(\hat{\mathbf{x}}^i - \text{step}^i \nabla_{\mathbf{x}} \|\mathbf{y} - \mathbf{A}\hat{\mathbf{x}}^i\|_2^2), \quad (3)$$

where  $\mathcal{P}_K(\cdot)$  is Euclidean projection on the  $K$ -sparse simplex,  $\hat{\mathbf{x}}^i$  is the iteration- $i$  estimate,  $\text{step}^i$  is iteration- $i$  the step size, and  $\nabla_{\mathbf{x}}$  is the gradient w.r.t  $\mathbf{x}$ . For algorithms of this sort, rigorous approximation guarantees of (3) can be derived when  $\mathbf{A}$  obeys the restricted isometry property [15]. Determining the best choice of  $K$ , however, can be difficult in practice.

In this paper, we propose two methods for recovering a linearly constrained NN sparse vector  $\mathbf{x}$  from noisy linear observations  $\mathbf{y}$  of the form (1), both of which are based on the Generalized Approximate Message Passing (GAMP) algorithm [16], an instance of loopy belief propagation that has close connections to primal-dual optimization algorithms [17]. When run in “max-sum” mode, GAMP can be used to solve optimization problems of the form  $\hat{\mathbf{x}} = \arg \min_{\mathbf{x}} \sum_{m=1}^M f_m([\mathbf{A}\mathbf{x}]_m) + \sum_{n=1}^N g_n(x_n)$ , where  $\hat{\mathbf{x}}$  can be interpreted as the *maximum a posteriori* (MAP) estimate of  $\mathbf{x}$  under the assumed signal prior (4) and likelihood (5):

$$p(\mathbf{x}) \propto \prod_{n=1}^N \exp(-g_n(x_n)) \quad (4)$$

$$p(\mathbf{y}|\mathbf{A}\mathbf{x}) \propto \prod_{m=1}^M \exp(-f_m([\mathbf{A}\mathbf{x}]_m)). \quad (5)$$

When run in “sum-product” mode, GAMP returns an approximation of the minimum mean-squared error (MMSE) estimate of  $\mathbf{x}$  under the same assumptions. In either case, the linear equality constraints  $\mathbf{B}\mathbf{x} = \mathbf{c}$  can be enforced through the use of noiseless pseudo-measurements, as described in the sequel.

The first of our proposed approaches solves (2) using max-sum GAMP while tuning  $\lambda$  using a novel expectation-maximization (EM) [18] procedure. We henceforth refer to this approach as EM-NNL-GAMP, where NNL is short for “non-

negative LASSO.<sup>1</sup> We demonstrate, via extensive numerical experiments, that 1) the *runtime* of our approach is much faster than the state-of-the-art TFOCS solver [21] for a fixed  $\lambda$ , and that 2) the MSE *performance* of our  $\lambda$ -tuning procedure is on par with TFOCS under *oracle* tuning. We also consider the special case of  $\lambda=0$ , yielding “non-negative least squares GAMP” (NNLS-AMP), whose performance and runtime compare favorably to Matlab’s `lsqlin` routine. In addition, we consider a variation on (2) that replaces the quadratic loss  $\frac{1}{2}\|\mathbf{y} - \mathbf{A}\mathbf{x}\|_2^2$  with the absolute loss  $\|\mathbf{y} - \mathbf{A}\mathbf{x}\|_1$  for improved robustness to outliers in  $\mathbf{w}$  [22], and demonstrate the potential advantages of this technique on a practical dataset.

The second of our proposed approaches aims to solve not an optimization problem like (2) but rather an inference problem: compute the *MMSE estimate* of a linearly constrained NN sparse vector  $\mathbf{x}$  from noisy linear observations  $\mathbf{y}$ . This is in general a daunting task, since computing the true MMSE estimate requires i) knowing both the true signal prior  $p(\mathbf{x})$  and likelihood  $p(\mathbf{y}|\mathbf{A}\mathbf{x})$ , which are rarely available in practice, and ii) performing optimal inference w.r.t that prior and likelihood, which is rarely possible in practice for computational reasons.

However, when the coefficients in  $\mathbf{x}$  are i.i.d and the observation matrix  $\mathbf{A}$  in (1) is sufficiently large and random, recent work [23] has demonstrated that near-MMSE estimation is indeed possible via the following methodology: place an i.i.d Gaussian-mixture (GM) model with parameters  $\mathbf{q}$  on the coefficients  $\{x_n\}$ , run sum-product GAMP based on that model, and tune the model parameters  $\mathbf{q}$  using an appropriately designed EM algorithm. For such  $\mathbf{A}$ , the asymptotic optimality of GAMP as an MMSE-inference engine was established in [16], [24], and the ability of EM-GAMP to achieve consistent estimates of  $\mathbf{q}$  was established in [25].

In this work, we show that the EM-GM-GAMP approach from [23] can be extended to *linearly constrained non-negative* signal models through the use of a non-negative Gaussian-mixture (NNGM) model and noiseless pseudo-measurements, and we detail the derivation and implementation of the resulting algorithm. Moreover, we demonstrate, via extensive numerical experiments, that EM-NNGM-GAMP’s reconstruction MSE is state-of-the-art and that its runtime compares favorably to existing methods.

Both of our proposed approaches can be classified as “empirical-Bayes” [26] in the sense that they combine Bayesian and frequentist approaches: GAMP performs (MAP or MMSE) Bayesian inference with respect to a given prior, where the parameters of the prior are treated as deterministic and learned using the EM algorithm, a maximum-likelihood (ML) approach.

*Notation:* For matrices, we use boldface capital letters like  $\mathbf{A}$ , and we use  $\mathbf{A}^\top$ ,  $\text{tr}(\mathbf{A})$ , and  $\|\mathbf{A}\|_F$  to denote the transpose, trace, and Frobenius norm, respectively. For vectors, we use boldface small letters like  $\mathbf{x}$ , and we use  $\|\mathbf{x}\|_p = (\sum_n |x_n|^p)^{1/p}$  to denote the  $\ell_p$  norm, with  $x_n = [\mathbf{x}]_n$  representing the  $n^{\text{th}}$  element of  $\mathbf{x}$ . Deterministic quantities

<sup>1</sup>In the absence of the constraint  $\mathbf{B}\mathbf{x} = \mathbf{c}$ , the optimization problem (2) can be recognized as a non-negatively constrained version of the LASSO [19] (also known as basis-pursuit denoising [20]). Similarly, in the special case of  $\lambda=0$ , (2) reduces to non-negative LS [14].

are denoted using serif typeface (e.g.,  $x, \mathbf{x}, \mathbf{X}$ ), while random quantities are denoted using san-serif typeface (e.g.,  $\mathbf{x}, \mathbf{X}, \mathbf{X}$ ). For random variable  $\mathbf{x}$ , we write the pdf as  $p_{\mathbf{x}}(x)$ , the expectation as  $\mathbb{E}\{\mathbf{x}\}$ , and the variance as  $\text{var}\{\mathbf{x}\}$ . For a Gaussian random variable  $\mathbf{x}$  with mean  $m$  and variance  $v$ , we write the pdf as  $\mathcal{N}(x; m, v)$  and, for the special case of  $\mathcal{N}(x; 0, 1)$ , we abbreviate the pdf as  $\varphi(x)$  and write the complimentary cdf as  $\Phi_c(x)$ . Meanwhile, for a Laplacian random variable  $\mathbf{x}$  with location  $m$  and scale  $v$ , we write the pdf as  $\mathcal{L}(x; m, v)$ . For the point mass at  $x = 0$ , we use the Dirac delta distribution  $\delta(x)$ . Finally, we use  $\mathbb{R}$  for the real field and  $\int_+ f(x)dx$  for the integral of  $f(x)$  over  $x \in [0, \infty)$ .

## II. GAMP OVERVIEW

As described in Sec. I, the generalized approximate message passing (GAMP) algorithm [16] is an inference algorithm capable of computing either MAP or approximate-MMSE estimates of  $\mathbf{x} \in \mathbb{R}^N$ , a realization of random vector  $\mathbf{x}$  with a prior pdf of the form (6), from generalized-linear observations  $\mathbf{y} \in \mathbb{R}^M$  that yield a likelihood of the form (7):

$$p_{\mathbf{x}}(\mathbf{x}) \propto \prod_{n=1}^N p_{x_n}(x_n) \quad (6)$$

$$p_{\mathbf{y}|\mathbf{z}}(\mathbf{y} | \mathbf{A}\mathbf{x}) \propto \prod_{m=1}^M p_{y_m|z_m}(y_m | [\mathbf{A}\mathbf{x}]_m), \quad (7)$$

where  $\mathbf{z} \triangleq \mathbf{A}\mathbf{x}$  represents “noiseless” transform outputs.

GAMP generalizes Donoho, Maleki, and Montanari’s Approximate Message Passing (AMP) algorithms [27], [28] from the case of AWGN-corrupted linear observations to the generalized-linear model (7). As we shall see, this generalization is useful when enforcing the linear equality constraints  $\mathbf{B}\mathbf{x} = \mathbf{c}$  and when formulating non-quadratic variations of (2).

GAMP is derived from particular approximations of loopy belief propagation (based on Taylor-series and central-limit-theorem arguments) that yield computationally simple “first-order” algorithms bearing strong similarity to primal-dual algorithms [17]. Importantly, GAMP admits rigorous analysis in the large-system limit (i.e.,  $M, N \rightarrow \infty$  for fixed ratio  $M/N$ ) under i.i.d zero-mean sub-Gaussian  $\mathbf{A}$  [16], [24], where its iterations obey a state evolution whose fixed points are optimal whenever they are unique. Meanwhile, for finite-sized problems and generic  $\mathbf{A}$ , max-sum GAMP yields the MAP solution when it converges, whereas sum-product GAMP minimizes a certain mean-field variational objective [17]. Although performance guarantees for generic finite-dimensional  $\mathbf{A}$  are lacking, in-depth empirical studies exist suggesting that (G)AMP performs relatively well for the  $\mathbf{A}$  typically used in compressive sensing applications [29].

Table I summarizes the GAMP algorithm. Effectively, GAMP converts the (computationally intractable) high-dimensional vector inference problem to a sequence of scalar inference problems. In this way, the complexity becomes dominated by four<sup>2</sup> matrix-vector multiplies per iteration: steps (R1), (R2), (R9), (R10), although even these steps become relatively cheap when the matrix-vector multiplies can be implemented using a fast transform. In the case of max-sum

<sup>2</sup>Two matrix multiplies per iteration, those in (R1) and (R9), can be eliminated using the “scalar variance” modification of GAMP, with vanishing degradation in the large-system limit [16].

inputs: $\forall m, n : p_{x_n}, p_{y_m z_m}, A_{mn}, T_{\max}, \epsilon_{\text{gamp}} > 0, \text{MaxSum} \in \{0, 1\}$
definitions:
$p_{z_m p_m}(z   \hat{p}; \mu^p) \triangleq \frac{p_{y_m z_m}(y_m z) \mathcal{N}(z; \hat{p}, \mu^p)}{\int_z p_{y_m z_m}(y_m z) \mathcal{N}(z; \hat{p}, \mu^p)} \quad (\text{D1})$
$p_{x_n r_n}(x   \hat{r}; \mu^r) \triangleq \frac{p_{x_n}(x) \mathcal{N}(x; \hat{r}, \mu^r)}{\int_x p_{x_n}(x) \mathcal{N}(x; \hat{r}, \mu^r)} \quad (\text{D2})$
initialize:
$\forall n : \hat{x}_n(1) = \int_x x p_{x_n}(x) \quad (\text{I1})$
$\forall n : \mu_n^x(1) = \int_x  x - \hat{x}_n(1) ^2 p_{x_n}(x) \quad (\text{I2})$
$\forall m : \hat{s}_m(0) = 0 \quad (\text{I3})$
for $t = 1 : T_{\max}$ ,
$\forall m : \mu_m^p(t) = \sum_{n=1}^N  A_{mn} ^2 \mu_n^x(t) \quad (\text{R1})$
$\forall m : \hat{p}_m(t) = \sum_{n=1}^N A_{mn} \hat{x}_n(t) - \mu_m^p(t) \hat{s}_m(t-1) \quad (\text{R2})$
if MaxSum then
$\forall m : \hat{z}_m(t) = \text{prox}_{-\ln p_{y_m z_m}}(\hat{p}_m(t); \mu_m^p(t)) \quad (\text{R3})$
$\forall m : \mu_m^z(t) = \mu_m^p(t) \text{prox}_{-\ln p_{y_m z_m}}(\hat{p}_m(t); \mu_m^p(t)) \quad (\text{R4})$
else
$\forall m : \hat{z}_m(t) = \text{E}\{z_m   p_m = \hat{p}_m(t); \mu_m^p(t)\} \quad (\text{R5})$
$\forall m : \mu_m^z(t) = \text{var}\{z_m   p_m = \hat{p}_m(t); \mu_m^p(t)\} \quad (\text{R6})$
end if
$\forall m : \mu_m^s(t) = (1 - \mu_m^z(t) / \mu_m^p(t)) / \mu_m^p(t) \quad (\text{R7})$
$\forall m : \hat{s}_m(t) = (\hat{z}_m(t) - \hat{p}_m(t)) / \mu_m^p(t) \quad (\text{R8})$
$\forall n : \mu_n^r(t) = \left( \sum_{m=1}^M  A_{mn} ^2 \mu_m^s(t) \right)^{-1} \quad (\text{R9})$
$\forall n : \hat{r}_n(t) = \hat{x}_n(t) + \mu_n^r(t) \sum_{m=1}^M A_{mn}^* \hat{s}_m(t) \quad (\text{R10})$
if MaxSum then
$\forall n : \hat{x}_n(t+1) = \text{prox}_{-\ln p_{x_n}}(\hat{r}_n(t); \mu_n^r(t)) \quad (\text{R11})$
$\forall n : \mu_n^x(t+1) = \mu_n^r(t) \text{prox}_{-\ln p_{x_n}}(\hat{r}_n(t); \mu_n^r(t)) \quad (\text{R12})$
else
$\forall n : \hat{x}_n(t+1) = \text{E}\{x_n   r_n = \hat{r}_n(t); \mu_n^r(t)\} \quad (\text{R13})$
$\forall n : \mu_n^x(t+1) = \text{var}\{x_n   r_n = \hat{r}_n(t); \mu_n^r(t)\} \quad (\text{R14})$
end if
if $\sum_{n=1}^N  \hat{x}_n(t+1) - \hat{x}_n(t) ^2 < \epsilon_{\text{gamp}} \sum_{n=1}^N  \hat{x}_n(t) ^2$ , break
end
outputs: $\forall m, n : \hat{z}_m(t), \mu_m^z(t), \hat{r}_n(t), \mu_n^r(t), \hat{x}_n(t+1), \mu_n^x(t+1)$

TABLE I  
THE GAMP ALGORITHM FROM [16] WITH MAX ITERATIONS  $T_{\max}$  AND STOPPING TOLERANCE  $\epsilon_{\text{GAMP}}$ .

GAMP, scalar inference is accomplished by lines (R3) and (R11) of Table I, which involve the proximal operator

$$\text{prox}_f(\hat{v}; \mu^v) \triangleq \arg \min_{x \in \mathbb{R}} f(x) + \frac{1}{2\mu^v} |x - \hat{v}|^2, \quad (8)$$

as well as lines (R4) and (R12), which involve the derivative of the prox operator with respect to the first argument. Meanwhile, in the case of sum-product GAMP, scalar inference is accomplished by lines (R5) and (R6), which compute the mean and variance of the iteration- $t$  approximations of the marginal posterior on  $Z_m$ ,

$$p_{z_m|p_m}(z | \hat{p}_m(t); \mu_m^p(t)) \propto p_{y_m|z_m}(y_m|z) \mathcal{N}(z; \hat{p}_m(t), \mu_m^p(t)), \quad (9)$$

as well as by lines (R13) and (R14), which compute the mean and variance of the approximate marginal posterior on  $x_n$ ,

$$p_{x_n|r_n}(x | \hat{r}_n(t); \mu_n^r(t)) \propto p_{x_n}(x) \mathcal{N}(x; \hat{r}_n(t), \mu_n^r(t)). \quad (10)$$

### III. OBSERVATION MODELS

To enforce the linear equality constraint  $\mathbf{B}\mathbf{x} = \mathbf{c}$  using GAMP, we extend the observation model (1) to

$$\begin{bmatrix} \mathbf{y} \\ \mathbf{c} \end{bmatrix} = \begin{bmatrix} \mathbf{A} \\ \mathbf{B} \end{bmatrix} \mathbf{x} + \begin{bmatrix} \mathbf{w} \\ \mathbf{0} \end{bmatrix} \quad (11)$$

and exploit the fact that GAMP supports a likelihood function that varies with the measurement index  $m$ . Defining  $\bar{\mathbf{y}} \triangleq [\mathbf{y}^T \mathbf{c}^T]^T$ ,  $\bar{\mathbf{A}} \triangleq [\mathbf{A}^T \mathbf{B}^T]^T$ , and  $\bar{\mathbf{z}} \triangleq \bar{\mathbf{A}}\mathbf{x}$ , the likelihood associated with the augmented model (11) can be written as

$$p_{\bar{\mathbf{y}}|\bar{\mathbf{z}}}(\bar{\mathbf{y}}|\bar{\mathbf{z}}) = \begin{cases} p_{y|z}(\bar{y}_m|\bar{z}_m) & m = 1, \dots, M \\ \delta(\bar{y}_m - \bar{z}_m) & m = M+1, \dots, M+P, \end{cases} \quad (12)$$

where  $p_{y|z}$  is the likelihood of the first  $M$  measurements (1).

Note that, for either max-sum or sum-product GAMP, the quantities in (R3)-(R6) then become

$$\hat{z}_m(t) = c_{m-M} \quad m = M+1, \dots, M+P, \quad (13)$$

$$\mu_m^z(t) = 0 \quad m = M+1, \dots, M+P. \quad (14)$$

#### A. Additive white Gaussian noise

When the noise  $\mathbf{w}$  is modeled as AWGN with variance  $\psi$ , the likelihood  $p_{y|z}$  in (12) takes the form

$$p_{y|z}(y|z) = \mathcal{N}(y; z, \psi). \quad (15)$$

In this case, for either max-sum or sum-product GAMP, the quantities in (R3)-(R6) of Table I become (omitting the  $t$  index for brevity)

$$\hat{z}_m = \hat{p}_m + \frac{\mu_m^p}{\mu_m^p + \psi} (y_m - \hat{p}_m) \quad m = 1, \dots, M \quad (16)$$

$$\mu_m^z = \frac{\mu_m^p \psi}{\mu_m^p + \psi} \quad m = 1, \dots, M. \quad (17)$$

#### B. Additive white Laplacian noise

The additive white Laplacian noise (AWLN) model presents an alternative to the AWGN model that is more robust to outliers [22]. For the Laplacian rate parameter  $\psi > 0$ , the likelihood  $p_{y|z}$  in (12) takes the form

$$p_{y|z}(y|z) = \mathcal{L}(y; z, \psi) \triangleq \frac{\psi}{2} \exp(-\psi|y - z|), \quad (18)$$

and so, for the max-sum case, (R3) in Table I becomes

$$\hat{z}_m = \arg \min_{z_m} |z_m - y_m| + \frac{(z_m - \hat{p}_m)^2}{2\mu_m^r \psi}. \quad (19)$$

The solution to (19) is quickly recognized as a  $y_m$ -shifted version of ‘‘soft-thresholding’’ function, and so the max-sum quantities (R3) and (R4) become, using  $\tilde{p}_m \triangleq \hat{p}_m - y_m$ ,

$$\hat{z}_m = \begin{cases} \hat{p}_m - \psi \mu_m^p & \tilde{p}_m \geq \psi \mu_m^p \\ \hat{p}_m + \psi \mu_m^p & \tilde{p}_m \leq -\psi \mu_m^p \\ y_m & \text{else} \end{cases} \quad m = 1, \dots, M, \quad (20)$$

$$\mu_m^z = \begin{cases} 0 & \hat{z}_m = y_m \\ \mu_m^p & \text{else} \end{cases} \quad m = 1, \dots, M. \quad (21)$$

Meanwhile, the sum-product GAMP quantities (R5) and (R6) from Table I (i.e., the mean and variance of the GAMP approximated  $Z_m$  posterior (9)) become

$$\hat{z}_m = y_m + \frac{C_m}{C_m} \left( \underline{p}_m - \sqrt{\mu_m^p} f(\underline{\kappa}_m) \right) + \frac{\bar{C}_m}{C_m} \left( \bar{p}_m + \sqrt{\mu_m^p} f(\bar{\kappa}_m) \right) \quad (22)$$

$$\mu_m^z = \frac{C_m}{C_m} \left( \mu_m^p g(\underline{\kappa}_m) + \left( \underline{p}_m - \sqrt{\mu_m^p} f(\underline{\kappa}_m) \right)^2 \right) + \frac{\bar{C}_m}{C_m} \left( \mu_m^p g(\bar{\kappa}_m) + \left( \bar{p}_m + \sqrt{\mu_m^p} f(\bar{\kappa}_m) \right)^2 \right) - (y_m - \hat{z}_m)^2, \quad (23)$$

where  $\underline{p}_m \triangleq \tilde{p}_m + \psi \mu_m^p$ ,  $\bar{p}_m \triangleq \tilde{p}_m - \psi \mu_m^p$ ,

$$\underline{C}_m \triangleq \frac{\psi}{2} \exp\left(\psi + \frac{1}{2}\psi^2 \mu_m^p\right) \Phi_c(\underline{\kappa}_m) \quad (24)$$

$$\bar{C}_m \triangleq \frac{\psi}{2} \exp\left(-\psi + \frac{1}{2}\psi^2 \mu_m^p\right) \Phi_c(\bar{\kappa}_m), \quad (25)$$

$C_m \triangleq \underline{C}_m + \bar{C}_m$ ,  $\underline{\kappa}_m \triangleq \underline{p}_m / \sqrt{\mu_m^p}$ ,  $\bar{\kappa}_m \triangleq -\bar{p}_m / \sqrt{\mu_m^p}$  and

$$f(a) \triangleq \frac{\varphi(a)}{\Phi_c(a)} \quad (26)$$

$$g(a) \triangleq 1 - f(a)(f(a) - a). \quad (27)$$

Derivations of (22) and (23) can be found in Appendix A-A.

#### IV. NON-NEGATIVE GAMP

##### A. NN Least Squares GAMP

We first detail the NNLS-AMP algorithm, which uses max-sum GAMP to solve the  $\lambda = 0$  case of (2). In this case, we want the cost function to reflect an infinite penalty when  $x_n < 0$  and no penalty when  $x_n \geq 0$ . To do so, we model the elements of  $\mathbf{x}$  as i.i.d from the (improper) NN prior pdf

$$p_{\mathbf{x}}(x) = \begin{cases} 1 & x \geq 0 \\ 0 & x < 0 \end{cases}. \quad (28)$$

Assuming AWGN, the i.i.d NN prior (28), and the augmented model (11), the max-sum GAMP estimate  $\hat{\mathbf{x}}$  obeys

$$\hat{\mathbf{x}} = \arg \min_{\mathbf{x}} - \sum_{n=1}^N \ln \mathbb{1}_{\mathbb{R}_+}(x_n) - \ln \mathbb{1}_{\mathbf{B}\mathbf{x}=\mathbf{c}}(\mathbf{x}) + \|\mathbf{y} - \mathbf{A}\mathbf{x}\|_2^2, \quad (29)$$

where  $\mathbb{1}_A(\cdot)$  is the indicator function on the set  $A$ . Hence, we see that (29) is equivalent to (2) when  $\lambda = 0$ .

Under the i.i.d NN uniform prior (28), it is readily shown that the max-sum GAMP steps (R11) and (R12) become

$$\hat{x}_n = \begin{cases} 0 & \hat{r}_n \leq 0 \\ \hat{r}_n & \hat{r}_n > 0 \end{cases}, \quad (30)$$

$$\mu_n^x = \begin{cases} 0 & \hat{r}_n \leq 0 \\ \mu_n^r & \hat{r}_n > 0 \end{cases}. \quad (31)$$

##### B. NN LASSO GAMP

Next we detail the NNL-AMP algorithm, which uses max-sum GAMP to solve the  $\lambda > 0$  case of (2). For this, we assume AWGN (15) (with variance  $\psi = \frac{1}{2}$ ), the augmented model (12), and  $\mathbf{x}$  with i.i.d exponential entries from the pdf

$$p_{\mathbf{x}}(x) = \begin{cases} -\lambda \exp(-\lambda x) & x \geq 0 \\ 0 & \text{else} \end{cases}. \quad (32)$$

It is then straightforward to show that the max-sum lines (R11) and (R12) in Table I reduce to

$$\hat{x}_n = \begin{cases} \hat{r}_n - \lambda \mu_n^r & \hat{r}_n \geq \lambda \mu_n^r \\ 0 & \text{else} \end{cases}, \quad (33)$$

$$\mu_n^x = \begin{cases} \mu_n^r & \hat{r}_n \geq \lambda \mu_n^r \\ 0 & \text{else} \end{cases}. \quad (34)$$

##### C. NN Gaussian Mixture GAMP

Finally, we detail the NNGM-GAMP algorithm, which employs sum-product GAMP under the i.i.d Bernoulli non-negative Gaussian mixture (NNGM) signal prior pdf

$$p_{\mathbf{x}}(x) = (1 - \tau)\delta(x) + \tau \sum_{\ell=1}^L \omega_{\ell} \mathcal{N}_+(x; \theta_{\ell}, \phi_{\ell}), \quad (35)$$

where  $\mathcal{N}_+(\cdot)$  denotes the non-negative Gaussian pdf, i.e.,

$$\mathcal{N}_+(x; \theta, \phi) = \begin{cases} \frac{\mathcal{N}(x; \theta, \phi)}{\Phi_c(-\theta/\sqrt{\phi})} & x \geq 0 \\ 0 & x < 0 \end{cases}, \quad (36)$$

$\tau \in (0, 1]$  is the sparsity rate, and  $\omega_{\ell}$ ,  $\theta_{\ell}$ , and  $\phi_{\ell}$  are the weight, location, and scale, respectively, of the  $\ell^{\text{th}}$  mixture component. For now, we treat the NNGM parameters  $[\tau, \boldsymbol{\omega}, \boldsymbol{\theta}, \boldsymbol{\phi}]$  and model order  $L$  as fixed and known.

Given the GAMP approximated posterior (10), the sum-product GAMP quantities (R13) and (R14) are (see Appendix B-A)

$$\hat{x}_n = \frac{\tau}{\zeta_n} \sum_{\ell=1}^L \beta_{n,\ell} (\gamma_{n,\ell} + \sqrt{\nu_{n,\ell}} f(\alpha_{n,\ell})), \quad (37)$$

$$\mu_n^x = \frac{\tau}{\zeta_n} \sum_{\ell=1}^L \beta_{n,\ell} \left( \nu_{n,\ell} g(\alpha_{n,\ell}) + (\gamma_{n,\ell} + \sqrt{\nu_{n,\ell}} f(\alpha_{n,\ell}))^2 \right) - \hat{x}_n^2, \quad (38)$$

with normalization factor

$$\zeta_n \triangleq (1 - \tau) \mathcal{N}(0; \hat{r}_n, \mu_n^r) + \tau \sum_{\ell=1}^L \beta_{n,\ell}. \quad (39)$$

The functions  $f(\cdot)$  and  $g(\cdot)$  are defined in (26) and (27), respectively, and the remaining quantities are

$$\alpha_{n,\ell} \triangleq \frac{-\gamma_{n,\ell}}{\sqrt{\nu_{n,\ell}}} \quad (40)$$

$$\gamma_{n,\ell} \triangleq \frac{\hat{r}_n / \mu_n^r + \theta_{\ell} / \phi_{\ell}}{1 / \mu_n^r + 1 / \phi_{\ell}}, \quad (41)$$

$$\nu_{n,\ell} \triangleq \frac{1}{1 / \mu_n^r + 1 / \phi_{\ell}} \quad (42)$$

$$\beta_{n,\ell} \triangleq \frac{\omega_{\ell} \mathcal{N}(\hat{r}_n; \theta_{\ell}, \mu_n^r + \phi_{\ell}) \Phi_c(\alpha_{n,\ell})}{\Phi_c(-\theta_{\ell} / \sqrt{\phi_{\ell}})}. \quad (43)$$

From (10), it can be shown that GAMP's approximation to the posterior activity probability  $\Pr\{\mathbf{x}_n \neq 0 | \mathbf{y}\}$  is

$$\pi_n = \frac{1}{1 + \left( \frac{\tau}{1 - \tau} \sum_{\ell=1}^L \beta_{n,\ell} \right)^{-1}}. \quad (44)$$

#### V. EM LEARNING OF THE PRIOR PARAMETERS

In the sequel, we will use  $\mathbf{q}$  to refer to the collection of prior parameters. For example, when NNGM-GAMP is used with the AWGN observation model,  $\mathbf{q} = [\tau, \boldsymbol{\omega}, \boldsymbol{\theta}, \boldsymbol{\phi}, \psi]$ . Since the value of  $\mathbf{q}$  that best fits the true data is typically unknown, we propose to learn it using an EM procedure [18]. The EM algorithm is an iterative technique that is guaranteed to converge to a local maximum (or a saddle point [30]) of the likelihood  $p(\mathbf{y}; \mathbf{q})$ .

To understand the EM algorithm, it is convenient to write the log-likelihood as [23]

$$\ln p(\mathbf{y}; \mathbf{q}) = \mathcal{Q}_{\hat{p}}(\mathbf{y}; \mathbf{q}) + D(\hat{p} \| p_{\mathbf{x}|\mathbf{y}}(\cdot | \mathbf{y}; \mathbf{q})), \quad (45)$$

where  $\hat{p}$  is an arbitrary distribution on  $\mathbf{x}$ ,  $D(\hat{p} \| \hat{q})$  is the Kullback-Leibler (KL) divergence between  $\hat{p}$  and  $\hat{q}$ , and

$$\mathcal{Q}_{\hat{p}}(\mathbf{y}; \mathbf{q}) \triangleq E_{\hat{p}}\{\ln p_{\mathbf{x},\mathbf{y}}(\mathbf{x}, \mathbf{y}; \mathbf{q})\} + H(\hat{p}), \quad (46)$$

where  $H(\hat{p})$  is the entropy of  $\mathbf{x} \sim \hat{p}$ . Importantly, the non-negativity of KL divergence implies that  $\mathcal{Q}_{\hat{p}}(\mathbf{y}; \mathbf{q})$  is a lower bound on (45). Starting from the initialization  $\mathbf{q}^0$ , the EM algorithm iteratively improves its estimate  $\mathbf{q}^i$  at each iteration  $i \in \mathbb{N}$ : first, it assigns  $\hat{p}^i(\cdot) = p_{\mathbf{x}|\mathbf{y}}(\cdot | \mathbf{y}; \mathbf{q}^i)$  to tighten the bound, and then it sets  $\mathbf{q}^{i+1}$  to maximize (46) with  $\hat{p} = \hat{p}^i$ .

Since the exact posterior pdf  $p_{\mathbf{x}|\mathbf{y}}(\cdot | \mathbf{y}; \mathbf{q}^i)$  is difficult to calculate, in its place we use GAMP's approximate posterior  $\prod_n p_{x_n|\tau_n}(\cdot | \hat{r}_n; \mu_n^r; \mathbf{q}^i)$  from (10), resulting in the EM update

$$\mathbf{q}^{i+1} = \arg \max_{\mathbf{q}} \hat{\mathbb{E}}\{\ln p(\mathbf{x}, \mathbf{y}; \mathbf{q}) | \mathbf{y}; \mathbf{q}^i\}, \quad (47)$$

where  $\hat{\mathbb{E}}$  denotes expectation using GAMP's approximate posterior. Also, because calculating the joint update for  $\mathbf{q}$  in (47) can be difficult, we perform the maximization (47) one component at a time, known as "incremental EM" [31]. Note that, even when using an approximate posterior and updating incrementally, the EM algorithm iteratively maximizes a lower-bound to the log-likelihood. Also note that the sum-product approximate posteriors (10) are used even when tuning (the max-sum-GAMP based) NNL-GAMP.

Next, we provide details on the EM updates (47) for various prior parameters. Since, however, the updates of the AWGN noise variance  $\psi$  [recall (15)] and the the NNGM sparsity rate  $\tau$  [recall (35)] are identical to those described in [23], we do not describe them below.

#### A. EM update of Laplacian rate parameter

We first derive the EM updates of the Laplacian likelihood's rate parameter  $\psi$  [recall (18)]. Because we can write  $p(\mathbf{x}, \mathbf{y}; \mathbf{q}) = D \prod_{m=1}^M p_{y|z}(y_m | z_m; \psi)$  for a  $\psi$ -invariant constant  $D$ , the incremental update of  $\psi$  from (47) becomes

$$\psi^{i+1} = \arg \max_{\psi > 0} \sum_{m=1}^M \hat{\mathbb{E}}\{\ln p_{y|z}(y_m; \mathbf{a}_m^T \mathbf{x}; \psi) | \mathbf{y}; \mathbf{q}^i\}. \quad (48)$$

In Appendix A-B, we show that (48) implies

$$\psi^{i+1} = M \left( \sum_{m=1}^M \mathbb{E}\{|z_m - y_m| | \mathbf{y}; \hat{p}_m, \nu_m^p \psi^i\} \right)^{-1}, \quad (49)$$

where

$$\begin{aligned} & \hat{\mathbb{E}}\{|z_m - y_m| | \mathbf{y}; \hat{p}_m, \nu_m^p, \psi^i\} \\ & \triangleq \frac{\bar{C}_m}{C_m} \left( \bar{p}_m + \sqrt{\mu_m^p} f(\bar{\kappa}_m) \right) - \frac{C_m}{C_m} \left( \underline{p}_m - \sqrt{\mu_m^p} f(\underline{\kappa}_m) \right), \end{aligned} \quad (50)$$

for  $C_m, \underline{C}_m, \bar{C}_m, \underline{p}_m, \bar{p}_m, \underline{\kappa}_m, \bar{\kappa}_m, f(\cdot)$  defined in Sec. III-B.

#### B. EM update of exponential rate parameter

Noting that  $p(\mathbf{x}, \mathbf{y}; \mathbf{q}) = D \prod_{n=1}^N p_{\mathbf{x}}(x_n; \lambda)$  for a  $\lambda$ -invariant constant  $D$ , the incremental EM update of the exponential rate parameter  $\lambda$  is

$$\lambda^{i+1} = \arg \max_{\lambda > 0} \sum_{n=1}^N \hat{\mathbb{E}}\{\ln p_{\mathbf{x}}(\mathbf{x}_n; \lambda) | \mathbf{y}; \lambda^i\}, \quad (51)$$

which reduces to

$$\lambda^{i+1} = N \left( \sum_{n=1}^N \tilde{r}_n + \sqrt{\mu_n^r} f\left(-\frac{\tilde{r}_n}{\sqrt{\mu_n^r}}\right) \right)^{-1} \quad (52)$$

for  $\tilde{r}_n \triangleq \hat{r}_n - \lambda \mu^r$ . The derivation of (52) closely follows the derivation of the Laplacian rate update (49) after replacing the "output" variables (e.g.,  $z_m$  and  $\hat{p}_m$ ) with the corresponding "input" variables (e.g.,  $x_n$  and  $\hat{r}_n$ ) and noting that the exponential pdf has support only on  $[0, \infty)$ . We emphasize that this procedure automatically "tunes" the regularization parameter  $\lambda$  in (2), a notoriously difficult problem (see, e.g., [13]).

#### C. EM updates for NNGM parameters and model-order selection

Noting that  $p(\mathbf{x}, \mathbf{y}; \mathbf{q}) = D \prod_{n=1}^N p_{\mathbf{x}}(x_n; \boldsymbol{\omega}, \boldsymbol{\theta}, \phi)$  for a  $[\boldsymbol{\omega}, \boldsymbol{\theta}, \phi]$ -invariant constant  $D$ , the incremental EM updates take the form

$$\boldsymbol{\theta}_k^{i+1} = \arg \max_{\boldsymbol{\theta}_k \in \mathbb{R}} \sum_{n=1}^N \hat{\mathbb{E}}\{\ln p_{\mathbf{x}}(\mathbf{x}_n; \boldsymbol{\theta}_k, \mathbf{q}_{\boldsymbol{\theta}_k}^i | \mathbf{y}; \mathbf{q}^i\}, \quad (53)$$

$$\phi_k^{i+1} = \arg \max_{\phi_k > 0} \sum_{n=1}^N \hat{\mathbb{E}}\{\ln p_{\mathbf{x}}(\mathbf{x}_n; \phi_k, \mathbf{q}_{\phi_k}^i | \mathbf{y}; \mathbf{q}^i\}, \quad (54)$$

$$\boldsymbol{\omega}^{i+1} = \arg \max_{\boldsymbol{\omega} > 0: \sum_k \omega_k = 1} \sum_{n=1}^N \hat{\mathbb{E}}\{\ln p_{\mathbf{x}}(\mathbf{x}_n; \boldsymbol{\omega}, \mathbf{q}_{\boldsymbol{\omega}}^i | \mathbf{y}; \mathbf{q}^i\}, \quad (55)$$

where we use " $\mathbf{q}_{\boldsymbol{\omega}}^i$ " to denote the vector  $\mathbf{q}^i$  with  $\boldsymbol{\omega}^i$  removed (and similar for the other parameters). As derived in Appendix B-B, the above updates can be approximated as

$$\boldsymbol{\theta}_k^{i+1} = \frac{\sum_{n=1}^N \pi_n \bar{\beta}_{n,k} (\gamma_{n,k} + \sqrt{\nu_{n,k}} f(\alpha_{n,k}))}{\sum_{n=1}^N \pi_n \bar{\beta}_{n,k}} \quad (56)$$

$$\begin{aligned} \phi_k^{i+1} &= \frac{\sum_{n=1}^N \pi_n \bar{\beta}_{n,k} (\gamma_{n,k} + \sqrt{\nu_{n,k}} f(\alpha_{n,k}) - \theta_k)^2}{\sum_{n=1}^N \pi_n \bar{\beta}_{n,k}} \\ &+ \frac{\sum_{n=1}^N \pi_n \bar{\beta}_{n,k} \nu_{n,k} g(\alpha_{n,k})}{\sum_{n=1}^N \pi_n \bar{\beta}_{n,k}} \end{aligned} \quad (57)$$

$$\omega_k^{i+1} = \frac{\sum_{n=1}^N \pi_n \bar{\beta}_{n,k}}{\sum_{n=1}^N \pi_n}, \quad (58)$$

where the  $i^{\text{th}}$  iteration-dependent quantities  $\gamma_{n,\ell}, \nu_{n,\ell}, \alpha_{n,\ell}$ , and  $\beta_{n,\ell}$  are defined in (41)-(43), and  $\bar{\beta}_{n,k} \triangleq \beta_{n,k} / \sum_{\ell} \beta_{n,\ell}$ . Since the quantities above are already computed by NNGM-GAMP, the EM tuning procedure does not significantly increase the complexity beyond that of NNGM-GAMP.

The number of components  $L$  in the NNGM model (35) can be selected using the standard penalized log-likelihood approach to model-order-selection [32], i.e., by maximizing

$$\ln p(\mathbf{y}; \hat{\mathbf{q}}_L) - \eta(L), \quad (59)$$

where  $\hat{\mathbf{q}}_L$  is the ML estimate of  $\mathbf{q}$  under the hypothesis  $L$  (for which we would use the EM estimate) and  $\eta(L)$  is a penalty term such as that given by the Bayesian information criterion (BIC). Since this model-order-selection procedure is identical to that proposed for EM-GM-AMP in [23], we refer interested readers to [23] for more details. In practice, we find that the fixed choice of  $L = 3$  performs sufficiently well (see Sec. VI).

#### D. EM initialization

A good EM initialization is essential to avoiding bad local minima. For EM-NNL-AMP, we suggest setting the exponential rate parameter  $\lambda^0 = 1$ , as it performed well on our experiments, as shown in Sec. VI.

For EM-NNGM-AMP, we suggest an initial sparsity rate of

$$\tau^0 = \min \left\{ \frac{M}{N} \rho_{\text{SE}} \left( \frac{M}{N} \right), 1 - \epsilon \right\} \quad (60)$$

where  $\epsilon > 0$  is set arbitrarily small and  $\rho_{\text{SE}}(\cdot)$  is the theoretical noiseless phase-transition-curve (PTC) for  $\ell_1$  recovery of sparse non-negative (SNN) signals, shown to have the closed-form expression

$$\rho_{\text{SE}}(\delta) = \max_{c \geq 0} \frac{1 - (1/\delta)[(1 + c^2)\Phi(-c) - c\varphi(c)]}{1 + c^2 - [(1 + c^2)\Phi(-c) - c\varphi(c)]} \quad (61)$$

in [27], where  $\Phi(\cdot)$  and  $\varphi(\cdot)$  denote the cdf and pdf of the standard normal distribution. We then propose to set the initial values of the NNGM weights  $\{\omega_\ell\}$ , locations  $\{\theta_\ell\}$ , and scales  $\{\phi_\ell\}$  at the values that best fit the uniform pdf on  $[0, \sqrt{3}\varphi^0]$ , which can be computed offline similar to the standard EM-based approach described in [33, p. 435]. Under the AWGN model (15), we propose to set the initial variance of the noise and signal, respectively, as

$$\psi^0 = \frac{\|\mathbf{y}\|_2^2}{(\text{SNR} + 1)M}, \quad \varphi^0 = \frac{\|\mathbf{y}\|_2^2 - M\psi^0}{\|\mathbf{A}\|_F^2 \tau^0}, \quad (62)$$

where, without knowledge of the true  $\text{SNR} \triangleq \|\mathbf{A}\mathbf{x}\|_2^2 / \|\mathbf{w}\|_2^2$ , we suggest using the value  $\text{SNR} = 100$ . Meanwhile, under the i.i.d Laplacian noise model (18), we suggest to initialize the rate as  $\psi^0 = 1$ .

## VI. NUMERICAL RESULTS

### A. Validation of NNLS-AMP and NNL-AMP

To demonstrate that NNLS-AMP and `lsqlin` (Matlab's solver of (2) with  $\lambda = 0$ ) have the same unique critical points  $\hat{\mathbf{x}}^*$ , we conducted a brief experiment. At each realization,  $\mathbf{x} \in \mathbb{R}^N$  was constructed with  $K$  nonzero elements  $\{\underline{x}_k\}_{k=1}^K$  (placed uniformly at random), drawn i.i.d from a symmetric Dirichlet distribution with concentration parameter  $a > 0$ , whose pdf can be written as

$$p(\underline{x}_1, \dots, \underline{x}_{K-1}) = \begin{cases} \frac{\Gamma(aK)}{\Gamma(a)^K} \prod_{k=1}^K \underline{x}_k^{a-1}, & \underline{x}_k \in [0, 1] \\ 0 & \text{else} \end{cases} \quad (63a)$$

$$p(\underline{x}_K | \underline{x}_1, \dots, \underline{x}_{K-1}) = \delta(1 - \underline{x}_1 - \dots - \underline{x}_K) \quad (63b)$$

where  $\Gamma(\cdot)$  is the gamma function. Using  $\mathbf{A}$  with i.i.d  $\mathcal{N}(0, M^{-1})$  entries under problem dimensions  $M = 250$  and  $N = 100$ , we varied  $a = [0.01, 1, 100]$  and  $\text{SNR} \triangleq \|\mathbf{A}\mathbf{x}\|_2^2 / \|\mathbf{w}\|_2^2 = [10, 100, 1000]$ . We then averaged the

	$a = 0.01$			$a = 1$			$a = 100$			
	NMSE	time		NMSE	time		NMSE	time		
		NNLS-AMP	lsqlin		NNLS-AMP	lsqlin		NNLS-AMP	lsqlin	
SNR	10	-170.4	0.035	0.206	-164.0	0.065	0.051	-145.3	0.075	0.008
	100	-171.0	0.034	0.203	-162.7	0.069	0.025	-164.5	0.074	0.008
	1000	-169.6	0.037	0.206	-163.7	0.071	0.013	-162.2	0.074	0.008

TABLE II  
AVERAGE COMPARATIVE  $\overline{\text{NMSE}}$  [dB] (NNLS-AMP VS. `LSQLIN`) AND AVERAGE RUNTIME [SEC] FOR SYMMETRIC DIRICHLET SIGNAL RECOVERY.

	$K = 50$			$K = 100$			$K = 150$			
	NMSE	time		NMSE	time		NMSE	time		
		NNL-AMP	TFOCS		NNL-AMP	TFOCS		NNL-AMP	TFOCS	
$\lambda$	0.01	-135.7	0.024	0.091	-139.9	0.025	0.119	-140.8	0.025	0.104
	0.001	-125.4	0.026	0.130	-122.9	0.026	0.148	-117.0	0.027	0.008
	0.0001	-113.2	0.035	0.256	-113.4	0.036	0.262	-112.4	0.036	0.292

TABLE III  
AVERAGE COMPARATIVE  $\overline{\text{NMSE}}$  [dB] (NNL-AMP VS. TFOCS) AND AVERAGE RUNTIME [SEC] FOR SYMMETRIC DIRICHLET SIGNAL RECOVERY.

comparative  $\overline{\text{NMSE}} \triangleq \|\hat{\mathbf{x}}_{\text{NNLS-AMP}} - \hat{\mathbf{x}}_{\text{lsqlin}}\|_2^2 / \|\mathbf{x}\|_2^2$  over  $R = 100$  realizations. Table II shows that NNLS-AMP and `lsqlin` return nearly the same estimates for all 9 SNR and concentration parameter combinations. Also, while `lsqlin` is slightly faster for  $a = 1$  and  $a = 100$ , we note that NNLS-AMP is faster for the sparse  $a = 0.01$  case. Though not shown here, we note that NNLS-AMP's complexity scales better with problem dimensions.

We then conducted a similar experiment comparing NNL-AMP to the Templates for First-Order Conic Solvers<sup>3</sup> (TFOCS) [21] algorithm for solving problem (2). Using  $\mathbf{A}$  with i.i.d  $\mathcal{N}(0, M^{-1})$  entries under problem dimensions  $M = 250$  and  $N = 100$ , we varied  $K = [50, 100, 150]$  and  $\|\cdot\|_1$  penalty  $\lambda = [10^{-2}, 10^{-3}, 10^{-4}]$ . At each realization,  $\mathbf{x} \in \mathbb{R}^N$  had  $K$ -sparse elements who were drawn from the symmetric Dirichlet distribution (63) with concentration parameter  $a = 1$  and the noise  $\mathbf{w}$  was AWGN such that  $\text{SNR} = 20$  dB. We then averaged the comparative  $\overline{\text{NMSE}} \triangleq \|\hat{\mathbf{x}}_{\text{NNL-AMP}} - \hat{\mathbf{x}}_{\text{TFOCS}}\|_2^2 / \|\mathbf{x}\|_2^2$  over  $R = 100$  realizations. Since TFOCS did not have a built in function to enforce the linear equality constraints, we did not do so with NNL-AMP. Table III shows that both algorithms converged to almost the same solutions as  $\overline{\text{NMSE}} < -110$  dB for all experiments. Moreover, NNL-AMP was much faster than TFOCS for all nine experiments.

### B. Noiseless Empirical Phase Transitions

First, we present empirically generated phase-transition curves (PTCs) for the recovery of  $K$ -sparse  $N$ -length simplex signals from  $M$  noiseless measurements.

To evaluate each PTC, we fixed  $N = 500$  and constructed a  $20 \times 20$  uniformly spaced grid on the  $\frac{M}{N}$ -versus- $\frac{K}{M}$  plane over the ranges  $\frac{M}{N} \in [0.05, 1]$  and  $\frac{K}{M} \in [0.05, 1]$ . At each grid point, we drew  $R = 100$  independent realizations of the pair  $(\mathbf{A}, \mathbf{x})$ , where  $\mathbf{A} \in \mathbb{R}^{M \times N}$  was constructed with i.i.d  $\mathcal{N}(0, M^{-1})$  entries and  $\mathbf{x} \in \mathbb{R}^N$  was constructed with  $K$  nonzero elements  $\{\underline{x}_k\}_{k=1}^K$  (placed uniformly at random),

<sup>3</sup>Matlab code is available at <http://cvxr.com/tfocs/download/>.

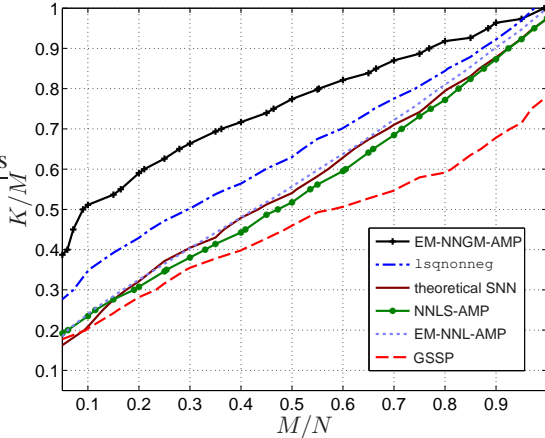


Fig. 1. Empirical PTCs and  $\ell_1$ -SNN theoretical PTC for noiseless recovery of length- $N = 500$ ,  $K$ -sparse, symmetric Dirichlet signals with concentration  $a = 1$  from  $M$  measurements.

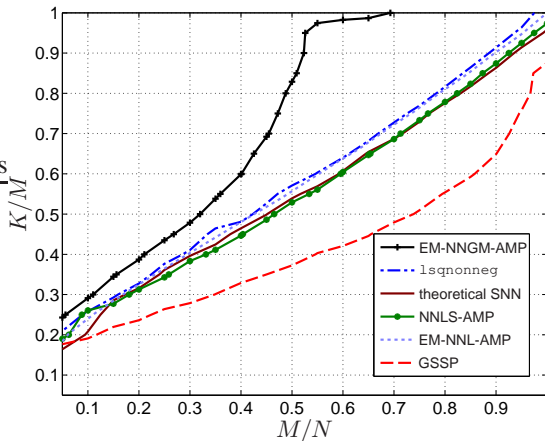


Fig. 2. Empirical PTCs and  $\ell_1$ -SNN theoretical PTC for noiseless recovery of length- $N = 500$ ,  $K$ -sparse, symmetric Dirichlet signals with concentration  $a = 100$  from  $M$  measurements.

drawn i.i.d from a symmetric Dirichlet distribution with concentration parameter  $a > 0$ , as shown in (63), which enforces the simplex constraint. For the  $r^{\text{th}}$  realization of  $(\mathbf{A}, \mathbf{x})$ , we then recovered  $\mathbf{x}$  from the noiseless observation  $\mathbf{y} = \mathbf{A}\mathbf{x}$  and defined the recovery  $\hat{\mathbf{x}}$  to be “successful” if  $\text{NMSE} \triangleq \|\mathbf{x} - \hat{\mathbf{x}}\|_2^2 / \|\mathbf{x}\|_2^2 < 10^{-6}$ . Using  $S_r = 1$  to mark a success and  $S_r = 0$  otherwise, the average success rate was then computed via  $\bar{S} \triangleq \frac{1}{R} \sum_{r=1}^R S_r$ , and the empirical PTC was then plotted as the  $\bar{S} = 0.5$  level-curve using Matlab’s contour command.

Figures 1–2 show the empirical PTCs for symmetric Dirichlet distributions with parameter  $a = 1$  (i.e., uniformly distributed over the simplex) and  $a = 100$  (i.e.,  $\underline{x}_k \approx \frac{1}{K} \forall k$ ), respectively, using the proposed “simplex EM-NNGM-AMP” approach, greedy selection and simplex projection (GSSP) [6], and Matlab’s `lsqnonneg` (using the augmented model (11)). We note that the simplex-enforcing `lsqlin` Matlab command was highly unstable in these problems. In addition, Figures 1–2 show the theoretical SNN  $\ell_1$ -recovery PTC  $\rho_{SE}(\frac{M}{N})$  from (61). For the GSSP algorithm, we initialized  $\hat{\mathbf{x}}^0$  as the SPGL1 [34] solution (using the augmented model from (11)) and set the step size as  $100/\|\mathbf{A}\|_F^2$ , as it yielded the best overall PTCs.

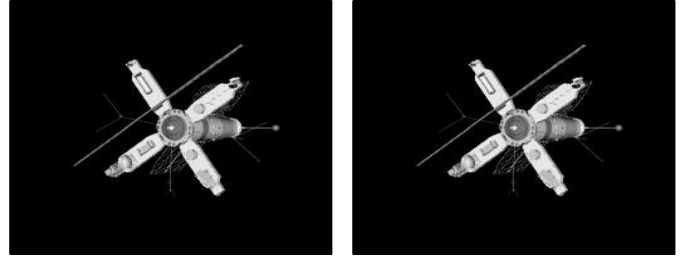


Fig. 3. Sparse non-negative image of a satellite: original image on left and EM-NNGM-AMP recovery at  $\frac{M}{N} = \frac{1}{4}$  on right.

Figures 1–2 show that the proposed simplex-EM-NNGM-AMP approach yields empirical PTCs that are significantly better than those of the competing approaches. Its excellent performance is the result of three factors: i) the generality of the NNGM prior, ii) the ability of the EM approach to accurately learn the prior parameters, and iii) the ability of GAMP to exploit the learned prior. In fact, Fig. 2 shows simplex-NNGM-AMP accurately reconstructing  $K$ -sparse signals from only  $M = K$  measurements even while  $N > M$ , thereby achieving a sort of “holy grail” in sparse reconstruction. The latter is possible because the signal  $\mathbf{x}$  is highly structured when  $a = 100$ , and because the proposed approach can learn and exploit that structure. While EM-NNL-AMP and NNLS-AMP did not perform nearly as well as EM-NNGM-AMP, we do note that they nearly matched the theoretical SNN  $\ell_1$ -recovery PTC for both signal types.

### C. Non-negative Image Recovery

As a practical example, we experimented with the recovery of a sparse non-negative image. For this, we used the  $N = 256 \times 256$  satellite image shown in Fig. 3, which contained  $K = 6678$  nonzero pixels and  $N - K = 58858$  zero-valued pixels, and thus was approximately 10% sparse. Linearly compressed measurements  $\mathbf{y} = \mathbf{A}\mathbf{x} + \mathbf{w}$  were collected under i.i.d Gaussian noise  $\mathbf{w}$  whose variance was selected to achieve  $\text{SNR} = 60$  dB. Here,  $\mathbf{x}$  represents the (rasterized) image and  $\mathbf{A}$  a linear measurement operator configured as  $\mathbf{A} = \Phi\Psi\mathbf{S}$ , where  $\Phi \in \{0, 1\}^{M \times N}$  was constructed from rows of the  $N \times N$  identity matrix selected uniformly at random,  $\Psi \in \{-1, 1\}^{N \times N}$  was a Hadamard transform, and  $\mathbf{S} \in \mathbb{R}^{N \times N}$  was a diagonal matrix with  $\pm 1$  diagonal entries chosen uniformly at random. Note that multiplication by  $\mathbf{A}$  can be executed using a fast binary algorithm, making it attractive for hardware implementation. For this experiment, no linear equality constraints exist and so the observation model was not augmented.

As a function of the sampling ratio  $\frac{M}{N}$ , Fig. 4 shows the NMSE and runtime averaged over  $R = 100$  realizations of  $\mathbf{A}$  and  $\mathbf{w}$  for the proposed EM-NNGM-AMP and EM-NNL-AMP in comparison to EM-GM-AMP from [23], genie-tuned non-negative LASSO via TFOCS [21],<sup>4</sup> and genie-tuned

<sup>4</sup>Using EM-NNL-AMP’s  $\hat{\mathbf{x}}$ , we ran TFOCS over an 11-point grid of hypothesized non-negative  $\ell_1$  penalty  $\lambda \in \{0.5\|\mathbf{A}^T(\mathbf{y} - \mathbf{A}\hat{\mathbf{x}})\|_\infty, \dots, 2\|\mathbf{A}^T(\mathbf{y} - \mathbf{A}\hat{\mathbf{x}})\|_\infty\}$  and then reported the total runtime and best NMSE.

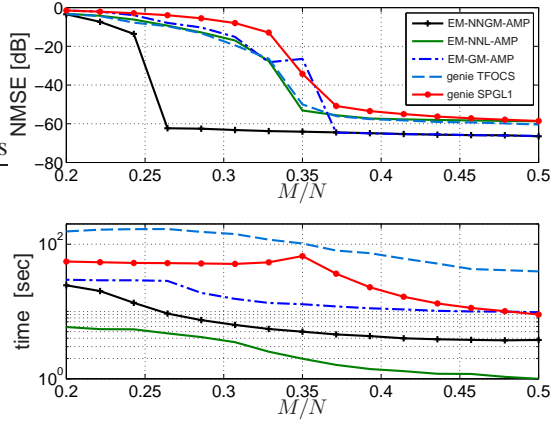


Fig. 4. Recovery NMSE (top) and runtime (bottom) versus  $\frac{M}{N}$  for the sparse NN satellite image for the proposed EM-NNGM-AMP and EM-NNL-AMP compared to EM-GM-AMP, non-negative LASSO via TFOCS, and standard LASSO via SPGL1.

standard LASSO implemented via SPGL1<sup>5</sup> [34]. Results for `lsqnonneg` are not shown because its per-realization runtime exceeded three hours (since `lsqnonneg` treats  $\mathbf{A}$  as an explicit matrix).

Figure 4 (top) shows that the proposed EM-NNGM-AMP algorithm provided the most accurate signal recoveries for all undersampling ratios. Remarkably, its phase-transition occurred at  $\frac{M}{N} \approx 0.25$ , whereas that of the other algorithms occurred at  $\frac{M}{N} \approx 0.35$ . The gain of EM-NNGM-AMP over EM-GM-AMP can be attributed to the former’s exploitation of signal non-negativity, whereas the gain of EM-NNGM-AMP over non-negative LASSO (either via EM-NNL-AMP or genie-tuned TFOCS) can be attributed to former’s learning/exploitation of the true signal distribution. Finally, the gain of non-negative LASSO over standard LASSO can be attributed to the former’s exploitation of signal non-negativity. In terms of runtime, EM-NNGM-AMP was about  $3\times$  as fast as EM-GM-AMP, between  $3\times$  to  $15\times$  as fast as standard LASSO (via SPGL1), and  $10\times$  to  $20\times$  as fast as non-negative LASSO (via TFOCS).

Finally, Fig. 4 (bottom) shows that the proposed EM-NNGM-AMP algorithm exhibited the second-fastest runtimes, showing that excellent recovery performance need not come at the expense of computational complexity. We accredit EM-NNL-AMP’s fastest runtimes to its ability to automatically tune its exponential rate parameter via EM, compared to the “hand-tuning” method of SPGL1.

### D. Portfolio Optimization

Given  $N$  securities, we denote  $\mathbf{r}_t = [r_{1t}, \dots, r_{Nt}]^\top$  as the  $N \times 1$  vector of returns at time  $t$ . Under the return-adjusted Markowitz mean-variances (MV) framework, the goal is to divide one unit of capital among the  $N$  securities (i.e., a *portfolio*) as to maximize future returns while minimizing the risk. Assuming stationary returns, the MV framework selects

<sup>5</sup>We ran SPGL1 in “BPDN mode,” i.e., solving  $\min_{\mathbf{x}} \|\mathbf{x}\|_1$  s.t.  $\|\mathbf{y} - \mathbf{A}\mathbf{x}\|_2 < \sigma$  for hypothesized tolerances  $\sigma^2 \in \{0.3, 0.6, \dots, 1.5\} \times M\psi$  and then reported the total runtime and best NMSE.

a portfolio  $\hat{\mathbf{x}}$  such that [3]

$$\hat{\mathbf{x}} = \arg \min_{\mathbf{x} \in \Delta^+} \|\rho \mathbf{1} - \mathbf{A}\mathbf{x}\|_2^2 \quad \text{s.t.} \quad \boldsymbol{\mu}^\top \mathbf{x} = \rho, \quad (64)$$

where  $\mathbf{1}$  is a vector of 1’s,  $\mathbf{A} = [\mathbf{r}_1, \dots, \mathbf{r}_T]^\top$ ,  $\boldsymbol{\mu} = \frac{1}{T} \sum_{t=1}^T \mathbf{r}_t$ , and  $\rho$  is the expected return.

However, in real-world scenarios, it was shown that the naïve strategy of dividing the assets equally (i.e.,  $x_n = \frac{1}{N} \forall n$ ) consistently outperformed several portfolio optimization algorithms assuming the MV framework [35]. There, DeMiguel et al. conjectured that the classic MV optimization technique was empirically unstable, where small changes in asset returns (among other factors) can have a profound impact on its estimates. Inspired by other regularization techniques, recent approaches have claimed to stabilize the procedure by adding an  $\ell_1$  penalty to the objective function (i.e., promoting sparsity), and have shown improved performance compared to the naïve strategy [4].

Using Fama and French 49 (FF49) industry portfolio database<sup>6</sup>, which consists of the monthly returns of  $N = 49$  securities from July 1971 to July 2011, we compared the NNLS-AMP, EM-NNL-AMP, EM-NNGM-AMP, `lsqlin`, and TFOCS cross-validation (CV)<sup>7</sup>, algorithms to the naïve strategy on the FF49 database. GSSP was not included in the study as the linear equality constraints  $\boldsymbol{\mu}^\top \mathbf{x} = \rho$  could not be guaranteed due to the simplex projector in (3).

For each algorithm, we set  $\rho = \rho_{\text{naïve}}$  and initialized the portfolios as the naïve strategy. For the `lsqnonneg`, we augmented the measurements via  $\bar{\mathbf{y}} \triangleq [\mathbf{y}, 500\rho]^\top$  and  $\bar{\mathbf{A}} = [\mathbf{A}, 500\boldsymbol{\mu}]^\top$ . For the TFOCS CV algorithm, we augmented the measurements via  $\bar{\mathbf{y}} \triangleq [\mathbf{y}, 500\rho, 500]^\top$  and  $\bar{\mathbf{A}} = [\mathbf{A}, 500\boldsymbol{\mu}, 500]^\top$ . To enforce the constraints in NNLS-AMP, EM-NNL-AMP, and EM-NNGM-AMP, we set  $\mathbf{B} = [\boldsymbol{\mu}, \mathbf{1}]^\top$  and  $\mathbf{c} = [\rho, 1]^\top$ , and augmented the system model. Lastly, we ran the three GAMP approaches under an AWGN likelihood (15) and an AWLN likelihood (18).

Starting from July 1981, we construct the  $i^{\text{th}}$  year’s portfolio  $\hat{\mathbf{x}}(i)$  for each algorithm given the previous 120 months of return data  $\mathbf{A}_{\text{train}} = [\mathbf{r}_{12(i-1)+1}, \dots, \mathbf{r}_{12(i-1)+120}]^\top$  and empirical mean return  $\hat{\boldsymbol{\mu}}_{\text{train}} = \frac{1}{120} \mathbf{A}_{\text{train}} \mathbf{1}$ . Then, we compute the statistics  $\hat{\rho}_{\text{test}}(i)$ ,  $\sigma_{\text{test}}^2(i)$ , given by

$$\hat{\rho}_{\text{test}}(i) = \frac{1}{12} \sum_{t=1}^{12} \hat{\mathbf{x}}(i)^\top \mathbf{r}_t, \quad (65)$$

$$\sigma_{\text{test}}^2(i) = \frac{1}{19} \sum_{t=1}^{12} (\hat{\mathbf{x}}(i)^\top \mathbf{r}_t - \hat{\rho}_{\text{test}})^2, \quad (66)$$

$$\text{SR}_{\text{test}}(i) = \frac{\hat{\rho}_{\text{test}}(i)}{\sigma_{\text{test}}(i)}, \quad (67)$$

We then averaged the Sharpe ratios (a measure of risk vs. return), average return error  $\text{MSE}_{\text{LE}}(i) \triangleq |\boldsymbol{\mu} \hat{\mathbf{x}}(i) - \rho|^2$ , and yearly runtimes and reported them in Table IV. We see that

<sup>6</sup> The FF49 database and other financial datasets can be obtained from [http://mba.tuck.dartmouth.edu/pages/faculty/ken.french/data\\_library.html](http://mba.tuck.dartmouth.edu/pages/faculty/ken.french/data_library.html).

<sup>7</sup>For TFOCS, we used 4-fold cross-validation to select the regularization term  $\lambda$  using a grid from hypothesized  $\lambda \in \{0.001, \dots, 0.1\}$  consisting of 15 points.

		SR	MSE <sub>LE</sub>	time
naïve		0.3135	$-\infty$	-
lsq <sub>lin</sub>		0.3724	-57.0	<b>0.05</b>
TFOCS CV		0.3747	-56.9	31.92
AWGN	NNLS-AMP	0.3724	-72.5	0.91
	EM-NNL-AMP	0.3724	-72.5	0.86
	EM-NNGM-AMP	0.3858	-49.2	3.83
AWLN	NNLS-AMP	0.3822	-52.9	1.06
	EM-NNL-AMP	0.3816	-55.0	1.03
	EM-NNGM-AMP	<b>0.3891</b>	-52.9	5.04

TABLE IV  
AVERAGE RUNTIMES (IN SECONDS), TEST SHARPE RATIOS  
 $\text{SR} \triangleq \frac{1}{30} \sum_{i=1}^{30} \text{SR}(i)_{\text{TEST}}$ , AND RETURN ERRORS  
 $\text{MSE}_{\text{LE}} \triangleq \frac{1}{30} \sum_{i=1}^{30} \text{MSE}_{\text{LE}}$  (IN DB) FOR THE FF49 DATASET.

Matlab’s `lsqlin` and AWGN NNLS-AMP and EM-NNL-AMP yielded average Sharpe ratios about 0.06 higher than the naïve strategy. Meanwhile, AWGN EM-NNGM-AMP’s average Sharpe ratios were 0.013 higher than those algorithms. The TFOCS-CV algorithm yielded only a slightly better average Sharpe ratio than EM-NNL-AMP, but at the cost of a much greater complexity. Additionally, we see that assuming the AWLN versions of the GAMP approaches resulted in better performance compared to their AWGN counterparts, with AWLN EM-NNGM-AMP yielding the highest overall average Sharpe ratio.

In terms of runtimes, Matlab’s `lsqlin` was by far the fastest, though all GAMP approaches yielded manageable runtimes. Lastly, we see that all algorithms approximately enforce the linear equality constraint  $\boldsymbol{\mu}^\top \mathbf{x} = \rho$  since all average return errors  $\text{MSE}_{\text{LE}} < -49$  dB.

### E. Hyperspectral Image Unmixing

In hyperspectral unmixing, the goal is to decompose a spectral dataset measured over  $M$  spectral bands and  $T = T_1 \times T_2$  pixels (across a 2-D scene), into  $N$  constituent material spectra (or “endmembers”) with corresponding spatial abundances. Under the macroscopic model [2], we write the received radiance data  $\mathbf{Y}$  as the bilinear model

$$\mathbf{Y} = \mathbf{A}\mathbf{X} + \mathbf{W} \in \mathbb{R}^{M \times T}, \quad (68)$$

where, with  $N$  materials, the columns of  $\mathbf{A} \in \mathbb{R}_+^{M \times N}$  are the non-negative (NN) endmembers, the rows of  $\mathbf{X} \in \mathbb{R}_+^{N \times T}$  are NN abundance maps, and  $\mathbf{W}$  is noise. When the endmembers  $\mathbf{A}$  are already known and  $\mathbf{W}$  is assumed to be AWGN, (68) can be viewed as a multi-measurement vector (MMV) extension of (1) since the fractional abundances obey the simplex constraint, i.e.,  $\mathbf{X} \geq 0$  and  $\sum_{n=1}^N x_{nt} = 1 \forall t$ .

We now test the algorithms on the SHARE 2012 Avon dataset<sup>8</sup> [36], which consists of  $M = 360$  spectral bands, ranging from 400-2450 nm (consisting of visible and near infrared (VNIR) and short wave infrared (SWIR) bands), taken over a large rural scene. We cropped the data to focus on an unmixing scene [37] consisting of the pure grass, dry sand, black felt, and white TyVek materials. To select the  $N = 4$  endmembers, we used the vertex component analysis (VCA)

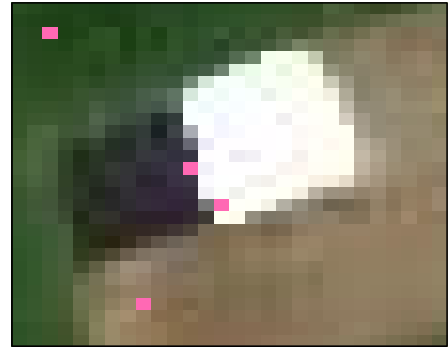


Fig. 5. RGB image of the cropped scene of the SHARE 2012 dataset [36]. The pixels corresponding to the VCA selected endmembers are pink.

algorithm [38]. The pixels corresponding to these endmembers are highlighted in pink in Fig. 5.

Fig. 6 shows the  $N = 4$  recovered abundance maps on the cropped SHARE 2012 dataset using the (a) NNLS-AMP, (b) EM-NNL-GAMP, (c) EM-NNGM-AMP, (d) fully constrained least squares (FCLS) algorithm [39], and (e) GSSP algorithms. For the EM-NNGM-AMP algorithm, we assumed an i.i.d  $L = 3$  component Bernoulli-NNGM prior for each row of  $\mathbf{X}$ , since the marginal abundance distributions are typically different across materials. Likewise, we learn each of the  $N = 4$  distributions’ parameters independently through EM. For GSSP, we assumed that each pixel was at most  $K = 3$  sparse, and selected a step size of  $\text{step}^i = 3/\|\mathbf{A}\|_F^2$ , as it yielded the best results.

All 4 algorithms recovered the white TyVek materials almost purely. Meanwhile, only EM-NNL-AMP was unable to recover a pure black felt material. In fact, from visual inspection, NNLS-AMP, FCLS, and GSSP recovered nearly identical abundance maps overall. However, EM-NNGM-AMP was able to estimate purer grass and dry sand abundances, as indicated by a deep red hues in the first two columns of Fig. 6-c. Meanwhile, FCLS was the fastest algorithm with a total runtime of 2.26 seconds, while the proposed NNLS-AMP, EM-NNL-AMP, and EM-NNGM-AMP were only slightly slower. GSSP was by far the slowest with a total runtime of just under 3 minutes.

Often times, the most difficult task is estimating the  $N$  endmembers from the hyperspectral radiance data  $\mathbf{Y}$ <sup>9</sup>. Though we used VCA to select the endmembers, there exists numerous other principled methods such as N-FINDR [40] or fast separable non-negative matrix factorization [41]. As an alternative, it is also possible to perform *joint* estimation of the endmembers  $\mathbf{A}$  and abundances  $\mathbf{X}$  using the bilinear generalized approximate message passing (BiG-AMP) algorithm [42], a recently proposed belief-propagation-based approach to matrix factorization. Moreover, EM-NNGM-AMP’s marginal abundance priors can be easily incorporated into the “turbo” message passing approach [43] (with BiG-AMP or GAMP), which leverages additional structures such as structured sparsity for improved abundance map estimation [44].

<sup>8</sup> The SHARE 2012 Avon dataset can be obtained from <http://www.rit.edu/cos/share2012/>.

<sup>9</sup>The model order selection problem of estimating the number of materials  $N$  is an important topic for future study.

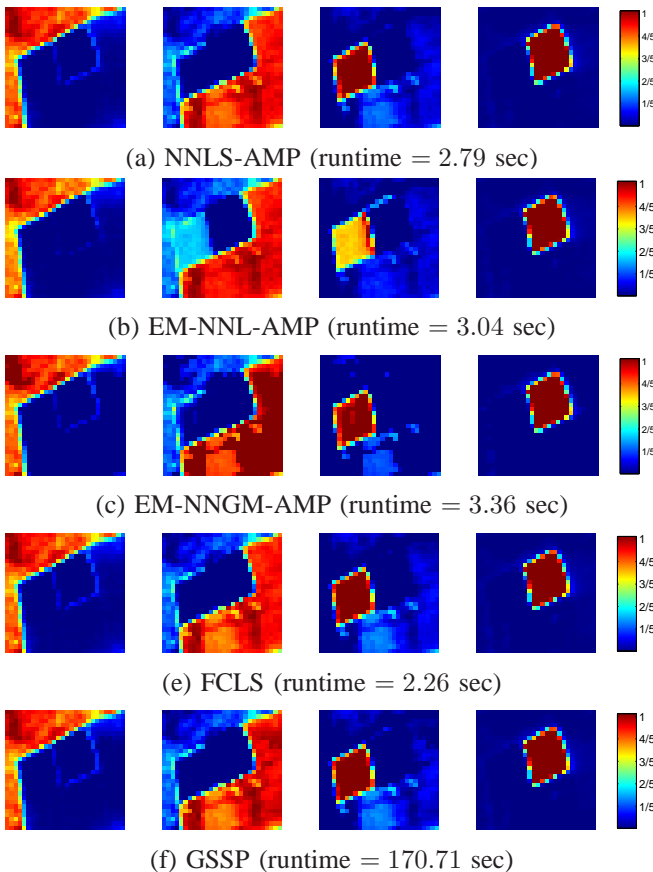


Fig. 6. The  $N = 4$  recovered abundance maps using the (b) US-GAMP, (c) EM-NNGM-GAMP, (e) FCLS, and (f) GSSP algorithms on the SHARE 2012 dataset using the selected endmembers. From left to right, the materials are: grass, dry sand, black felt, and white Tyvek. For visual comparison, Fig. 5, shows the color image of the scene.

#### ACKNOWLEDGMENTS

We would like to thank Jason Parker and Justin Ziniel for contributions to the Laplacian likelihood and EM-NNL-AMP.

#### VII. CONCLUSIONS

Recovering a linearly constrained NN sparse signal from noisy linear measurements arises in a plethora of applications. A natural approach is to formulate and solve a convex optimization problem that enforces these constraints. In this paper, we developed the NNLS-AMP and NNL-AMP algorithms that solved the convex problem (2) for the fixed  $\lambda = 0$  and  $\lambda > 0$  cases, respectively. Additionally, we developed a novel EM approach to automatically tune  $\lambda$ , as opposed to performing a computationally expensive cross-validation procedure that other solvers might use. Moreover, we developed the additive white Laplacian noise distribution for GAMP for use on data with known outliers.

Recently, an extensive numerical study on compressive sensing problems demonstrated the state-of-the-art performance of the empirical-Bayes technique EM-GM-AMP compared to many other well-known algorithms. Extending on this work, we proposed the EM-NNGM-AMP algorithm that assumes a flexible, sparsity-promoting i.i.d Bernoulli NNGM signal model, while simultaneously learning its parameters via EM. In addition, enforcing the linear equality constraints was

achieved via an augmented system model. The resulting EM-NNGM-AMP approach recovered the most accurate signal estimates on all tested experiments while exhibiting runtimes comparable to fast convex approaches.

#### APPENDIX A

##### DERIVATION OF LAPLACIAN LIKELIHOOD QUANTITIES

##### A. Laplacian likelihood steps for sum-product GAMP

Inserting the Laplacian likelihood (18) into the GAMP-approximated posterior (9), the GAMP update (R5) is (removing the  $m$  subscript for brevity)

$$\hat{z} \triangleq \mathbb{E}\{z | p = \hat{p}; \mu^r\} = \frac{1}{C} \int_z z \mathcal{L}(z; y; \psi) \mathcal{N}(z; \hat{p}, \mu^p) \quad (69)$$

where the scaling constant  $C$  is calculated as

$$C = \int_z \mathcal{L}(y; z, \psi) \mathcal{N}(z; \hat{p}, \mu^p) \quad (70)$$

$$= \int_z \mathcal{L}(z; 0, \psi) \mathcal{N}(z; \hat{p} - y, \mu^p) \quad (71)$$

$$= \underbrace{\frac{\psi}{2} \int_{-\infty}^0 \mathcal{N}(z; \tilde{p}, \mu^p) e^{\psi z} dz}_{\triangleq \underline{C}} + \underbrace{\frac{\psi}{2} \int_0^{\infty} \mathcal{N}(z; \tilde{p}, \mu^p) e^{-\psi z} dz}_{\triangleq \overline{C}} \quad (72)$$

We can compute  $\underline{C}$  and  $\overline{C}$  as (24) and (25), respectively, by completing the square inside the exponential terms in the integrands in (72) and simplifying.

Following similar techniques (i.e., shifting by  $y$  and splitting the integral), we see that (69) becomes

$$\hat{z} = y + \frac{\underline{C}}{C} \int_z z \mathcal{N}_-(z; \tilde{p}, \mu^p) + \frac{\overline{C}}{C} \int_z z \mathcal{N}_+(z; \tilde{p}, \mu^p), \quad (73)$$

where  $\mathcal{N}_+(\cdot)$  is defined in (36), and similarly,  $\mathcal{N}_-(x; a, b^2)$  is the Gaussian distribution with mean  $a$  and variance  $b^2$ , with truncated support on  $x \in (-\infty, 0]$  and scaled to unity. Supposing that  $u \sim \mathcal{N}(a, b^2)$ , [45] shows that

$$\mathbb{E}\{u | u > 0\} = \int_u \mathcal{N}_+(u; a, b^2) = a + b f\left(-\frac{a}{b}\right), \quad (74)$$

$$\mathbb{E}\{u | u < 0\} = \int_u u \mathcal{N}_-(u; a, b^2) = a - b f\left(\frac{a}{b}\right), \quad (75)$$

where  $f(\cdot)$  is defined in (26). Inserting (74) and (75) into (73), we get the MMSE-GAMP update (22).

To calculate the variance of the GAMP approximated posterior (9), we begin by calculating the second moment, i.e.,

$$\mathbb{E}\{z^2 | p = \hat{p}; \mu^p\} = \frac{1}{C} \int_z z^2 \mathcal{L}(z; y; \psi) \mathcal{N}(z; \hat{p}, \mu^p) \quad (76)$$

$$= \frac{1}{C} \int_z (z + y)^2 \mathcal{L}(z; 0; \psi) \mathcal{N}(z; \tilde{p}, \mu^p) \quad (77)$$

$$= 2y\hat{z} - y^2 + \frac{1}{C} \int_z z^2 \mathcal{L}(z; 0; \psi) \mathcal{N}(z; \tilde{p}, \mu^p) \quad (78)$$

$$= 2y\hat{z} - y^2 + \frac{1}{C} \left( \underline{C} \int z^2 \mathcal{N}_-(z; \tilde{p}, \mu^p) + \overline{C} \int z^2 \mathcal{N}_+(z; \tilde{p}, \mu^p) \right) \quad (79)$$

Given that  $\mathbf{u} \sim \mathcal{N}(a, b^2)$ , [45] shows that

$$\begin{aligned} \mathbb{E}\{\mathbf{u}^2 | \mathbf{u} > 0\} &= \text{var}\{\mathbf{u} | \mathbf{u} > 0\} + \mathbb{E}\{\mathbf{u} | \mathbf{u} > 0\}^2 \\ &= b^2 g(-\frac{a}{b}) + (a + bf(-\frac{a}{b}))^2, \end{aligned} \quad (80)$$

$$\begin{aligned} \mathbb{E}\{\mathbf{u}^2 | \mathbf{u} < 0\} &= \text{var}\{\mathbf{u} | \mathbf{u} < 0\} + \mathbb{E}\{\mathbf{u} | \mathbf{u} < 0\}^2 \\ &= b^2 g(\frac{a}{b}) + (a - bf(\frac{a}{b}))^2, \end{aligned} \quad (81)$$

where  $g(\cdot)$  is defined in (27). Inserting (80) and (81) into (79) and noting that  $\text{var}\{\mathbf{z} | \mathbf{p} = \hat{P}; \mu^p\} = \mathbb{E}\{\mathbf{z}^2 | \mathbf{p} = \hat{p}; \mu^p\} - \mathbb{E}\{\mathbf{z} | \mathbf{p} = \hat{p}; \mu^p\}^2$ , we obtain (23).

### B. EM update for Laplacian rate

Inserting the Laplacian likelihood (18) into (48), we see that the update for the Laplacian rate parameter  $\psi$  becomes.

$$\psi^{i+1} = \arg \max_{\psi} \hat{\mathbb{E}}\{\ln \mathcal{L}(y_m; z_m, \psi) | \mathbf{y}; \psi^i\} \quad (82)$$

$$= \arg \max_{\psi} M \ln \psi - \psi \sum_{m=1}^M \hat{\mathbb{E}}\{|z_m - y_m| | \mathbf{y}; \psi^i\}. \quad (83)$$

Zeroing the derivative of (83) w.r.t.  $\psi$ , we get the update (49). Finally, we see that the GAMP-approximated expectation is

$$\begin{aligned} &\hat{\mathbb{E}}\{|z_m - y_m| | \mathbf{y}; \hat{p}_m^p, \mu_m^p, \psi^i\} \\ &= \frac{1}{C_m^i} \int_{z_m} |z_m - y_m| \mathcal{L}(y_m; z_m, \psi^i) \mathcal{N}(z_m; \hat{p}_m, \nu_m^p) \quad (84) \end{aligned}$$

$$= \frac{1}{C_m^i} \int_{z_m} |z_m| \mathcal{L}(z_m; 0, \psi^i) \mathcal{N}(z_m; \tilde{p}_m, \mu_m^p) \quad (85)$$

Following similar techniques for deriving the MMSE-GAMP quantity (73), we get (50).

## APPENDIX B

### DERIVATION OF NNGM-GAMP QUANTITIES

#### A. Derivation of NNGM-GAMP MMSE estimates

Inserting the Bernoulli NNGM prior (35) into the GAMP approximated posterior (10), the posterior moment is calculated as (removing the subscript  $n$  notation for brevity)

$$\begin{aligned} \hat{x} &\triangleq \mathbb{E}_{\mathbf{x}|\mathbf{r}}\{\mathbf{x} | \mathbf{r} = \hat{\mathbf{r}}; \mu^r\} = \int_{\mathbf{x}} x p_{\mathbf{x}|\mathbf{r}}(x | \hat{\mathbf{r}}; \mu^r) \quad (86) \\ &= \frac{1}{\zeta} \int_{\mathbf{x}} x \mathcal{N}(x; \hat{r}, \mu^r) \left( (1 - \tau) \delta(x) + \tau \sum_{\ell=1}^L \omega_{\ell} \mathcal{N}_+(x; \theta_{\ell}, \phi_{\ell}) \right), \end{aligned}$$

where  $\zeta = \int_{\mathbf{x}} p_{\mathbf{x}}(x) \mathcal{N}(x; \hat{r}, \mu^r)$  is a scaling factor. Noting that the mean of the Dirac delta is zero, we see that

$$\hat{x} = \frac{\tau}{\zeta} \sum_{\ell=1}^L \omega_{\ell} \int_{\mathbf{x}} x \mathcal{N}(x; \hat{r}, \mu^r) \mathcal{N}_+(x; \theta_{\ell}, \phi_{\ell}), \quad (87)$$

where with the Gaussian-pdf multiplication rule<sup>10</sup> we get

$$\hat{x} = \frac{\tau}{\zeta} \sum_{\ell=1}^L \frac{\omega_{\ell} \mathcal{N}(\hat{r}; \theta_{\ell}, \mu^r + \phi_{\ell})}{\Phi_c(-\theta_{\ell}/\sqrt{\phi_{\ell}})} \int_{\mathbf{x}} x \mathcal{N}(x; \gamma_{\ell}, \nu_{\ell}), \quad (88)$$

where  $\gamma_{\ell}$  and  $\nu_{\ell}$  are defined in (41) and (42), respectively.

<sup>10</sup>  $\mathcal{N}(x; a, A) \mathcal{N}(x; b, B) = \mathcal{N}\left(x; \frac{a/A + b/B}{1/A + 1/B}, \frac{1}{1/A + 1/B}\right) \mathcal{N}(a; b, A+B)$ .

Using similar techniques, the normalization factor

$$\zeta = \int_{\mathbf{x}} \mathcal{N}(x; \hat{r}, \mu^r) \left( (1 - \tau) \delta(x) + \tau \sum_{\ell=1}^L \omega_{\ell} \mathcal{N}_+(x; \theta_{\ell}, \phi_{\ell}) \right) \quad (89)$$

can be shown to be equivalent to (39). Finally, using the mean of a truncated Gaussian (74), and inserting (39) into (88), we get the NNGM-GAMP estimate (37).

To calculate the variance of the GAMP approximated posterior (10), we note that

$$\begin{aligned} \mu^x &\triangleq \text{var}_{\mathbf{x}|\mathbf{r}}\{x | \hat{\mathbf{r}}; \mu^r\} \\ &= \int_{\mathbf{x}} x^2 p_{\mathbf{x}|\mathbf{r}}(x | \hat{\mathbf{r}}; \mu^r) - \mathbb{E}_{\mathbf{x}|\mathbf{r}}\{x | \mathbf{r} = \hat{\mathbf{r}}; \mu^r\}^2. \end{aligned} \quad (90)$$

Following (86)-(88) and using the Gaussian-pdf multiplication rule, we find the second moment to be

$$\int_{\mathbf{x}} x^2 p_{\mathbf{x}|\mathbf{r}}(x | \hat{\mathbf{r}}; \mu^r) = \frac{\tau}{\zeta} \sum_{\ell=1}^L \frac{\beta_{\ell}}{\Phi_c(\alpha_{\ell})} \int_{\mathbf{x}} x^2 \mathcal{N}(x; \gamma_{\ell}, \nu_{\ell}), \quad (91)$$

where  $\beta_{\ell}$  and  $\alpha_{\ell}$  are given in (43) and (40), respectively.

Leveraging the second moment of a truncated Gaussian (80) in (91), and then inserting (37) and (91) into (90), we obtain the NNGM-GAMP variance estimate (38).

#### B. EM updates of NNGM parameters

We first derive the EM update for  $\theta_k$ , the  $k^{\text{th}}$  component location, given the previous parameter estimate  $\mathbf{q}^i$ . The maximizing value of  $\theta_k$  in (53) is necessarily a value of  $\theta_k$  that zeros the derivative of the sum, i.e., that satisfies<sup>11</sup>

$$\frac{d}{d\theta_k} \sum_{n=1}^N \int_{x_n} p_{\mathbf{x}|\mathbf{r}}(x_n | \hat{\mathbf{r}}_n; \mu_n^r, \mathbf{q}^i) \ln p_{\mathbf{x}}(x_n; \theta_k, \mathbf{q}_{\theta_k}^i) = 0. \quad (92)$$

$$\Leftrightarrow \sum_{n=1}^N \int_{x_n} p_{\mathbf{x}|\mathbf{r}}(x_n | \hat{\mathbf{r}}_n; \mu_n^r, \mathbf{q}^i) \frac{d}{d\theta_k} \ln p_{\mathbf{x}}(x_n; \theta_k, \mathbf{q}_{\theta_k}^i) = 0. \quad (93)$$

For all  $x_n \geq 0$ , the derivative in (93) can be written as

$$\frac{d}{d\theta_k} \ln p_{\mathbf{x}}(x_n; \theta_k, \mathbf{q}_{\theta_k}^i) = \frac{\frac{d}{d\theta_k} \tau^i \omega_k^i \frac{\mathcal{N}(x_n; \theta_k; \phi_k^i)}{\Phi_c(-\theta_k/\sqrt{\phi_k^i})}}{p_{\mathbf{x}}(x_n; \theta_k, \mathbf{q}_{\theta_k}^i)}. \quad (94)$$

Unfortunately, plugging (94) into (93) yields an intractable integral, so we use the approximation<sup>12</sup>  $\Phi_c(-\theta_k/\sqrt{\phi_k^i}) \approx \Phi_c(-\theta_k^i/\sqrt{\phi_k^i})$ , yielding

$$\begin{aligned} \frac{d}{d\theta_k} \ln p_{\mathbf{x}}(x_n; \theta_k, \mathbf{q}_{\theta_k}^i) &= \left( \frac{x_n - \theta_k}{\phi_k^i} \right) \\ &\times \frac{\tau^i \omega_k^i \mathcal{N}(x_n; \theta_k; \phi_k^i) / \Phi_c(-\theta_k^i/\sqrt{\phi_k^i})}{(1 - \tau^i) \delta(x_n) + \tau^i (\omega_k^i \mathcal{N}_+(x_n; \theta_k; \phi_k^i) + \sum_{\ell \neq k} \omega_{\ell}^i \mathcal{N}_+(x_n; \theta_{\ell}^i, \phi_{\ell}^i))}. \end{aligned} \quad (95)$$

<sup>11</sup>By employing the Dirac approximation  $\delta(x) = \mathcal{N}(x; 0, \varepsilon)$  for fixed arbitrarily small  $\varepsilon > 0$ , the integrand and its derivative w.r.t  $\theta_k$  become continuous, justifying the exchange of differentiation and integration via the Leibniz integration rule. We apply the same reasoning for all exchanges of differentiation and integration in the sequel.

<sup>12</sup>This approximation becomes more accurate as  $\frac{d}{d\theta_k} \Phi_c(-\theta_k/\sqrt{\phi_k})$  tends to zero, i.e., when  $\theta_k/\sqrt{\phi_k}$  gets large. However, in our applications, this is typically the case since  $\phi_k \ll 1$  (since  $x_n \in [0, 1]$ ) and  $\theta_k > 0$ , i.e., only a small portion of the Gaussian tail is truncated to be non-zero.

We also note that (95) is zero at  $x_n = 0$  due to the Dirac delta function in the denominator.

Now, plugging in (95) and the approximated GAMP posterior  $p_{X|R}(x_n|\hat{r}_n; \mu_n^r, \mathbf{q}^i)$  from (10), integrating (93) separately over  $[\epsilon, \infty)$  and its complement, and taking  $\epsilon \rightarrow 0$ , we find that the  $(-\infty, \epsilon)$  portion vanishes, giving the necessary condition

$$\sum_{n=1}^N \int_+ \frac{p(x_n|x_n \neq 0, \mathbf{y}; \mathbf{q}^i) \omega_k^i \frac{\mathcal{N}(x_n; \theta_k, \phi_k^i)}{\Phi_c(-\theta_k^i/\sqrt{\phi_k^i})} (x_n - \theta_k)}{\zeta_n (\omega_k^i \mathcal{N}_+(x_n; \theta_k, \phi_k^i) + \sum_{\ell \neq k} \omega_\ell^i \mathcal{N}_+(x_n; \theta_\ell^i, \phi_\ell^i))} = 0, \quad (96)$$

where  $p(x_n|x_n \neq 0, \mathbf{y}; \mathbf{q}^i) \triangleq p_{X|R}(x_n|x_n \neq 0, \hat{r}_n; \mu_n^r, \mathbf{q}^i)$ . Since this integral cannot be evaluated in closed form, we apply the approximation  $\mathcal{N}(x_n; \theta_k, \phi_k^i) \approx \mathcal{N}(x_n; \theta_k^i, \phi_k^i)$  in both the numerator and denominator, and subsequently exploit the fact that, for  $x_n \geq 0$ ,  $p(x_n|x_n \neq 0, \mathbf{y}; \mathbf{q}^i) = \mathcal{N}(x_n; \hat{r}_n, \mu_n^r) \sum_{\ell} \omega_\ell^i \mathcal{N}_+(x_n; \theta_\ell^i, \phi_\ell^i)$  from (10) to cancel terms, where we obtain the necessary condition

$$\sum_{n=1}^N \int_+ \frac{\omega_k^i \mathcal{N}(x_n; \hat{r}_n, \mu_n^r) \mathcal{N}_+(x_n; \theta_k^i, \phi_k^i)}{\zeta_n} (x_n - \theta_k) = 0. \quad (97)$$

Now using the Gaussian-pdf multiplication rule, we get

$$\sum_{n=1}^N \frac{\beta_{n,k}}{\Phi_c(\alpha_{n,k})} \int_+ \mathcal{N}(x_n; \gamma_{n,k}, \nu_{n,k}) (x_n - \theta_k) = 0. \quad (98)$$

Following similar techniques as in Appendix B-A and noting that  $\beta_{n,k} = \pi_n \bar{\beta}_{n,k}$ , we see that the update  $\theta_k^{i+1}$  in (56) is the value of  $\theta_k$  that satisfies (98).

Similarly, the maximizing value of  $\phi_k$  in (54) is necessarily a value of  $\phi_k$  that zeroes the derivative, i.e.,

$$\sum_{n=1}^N \int_{x_n} p_{X|R}(x_n|\hat{r}_n; \mu_n^r, \mathbf{q}^i) \frac{d}{d\phi_k} \ln p_X(x_n; \phi_k, \mathbf{q}^i_{\phi_k}) = 0. \quad (99)$$

Using the prior given in (35), and simultaneously applying the approximation  $\Phi_c(-\theta_k^i/\sqrt{\phi_k}) \approx \Phi_c(-\theta_k^i/\sqrt{\phi_k^i})$ , we see that the derivative in (99) can be written as

$$\frac{d}{d\phi_k} \ln p_X(x_n; \phi_k, \mathbf{q}^i_{\phi_k}) = \frac{1}{2} \left( \frac{(x_n - \theta_k^i)^2}{\phi_k^2} - \frac{1}{\phi_k} \right) \times \frac{\tau^i \omega_k^i \mathcal{N}(x_n; \theta_k, \phi_k^i) / \Phi_c(-\theta_k^i/\sqrt{\phi_k^i})}{(1 - \tau^i) \delta(x_n) + \tau^i (\omega_k^i \mathcal{N}_+(x_n; \theta_k^i, \phi_k^i) + \sum_{\ell \neq k} \omega_\ell^i \mathcal{N}_+(x_n; \theta_\ell^i, \phi_\ell^i))}. \quad (100)$$

Integrating (99) separately over  $(-\infty, \epsilon)$  and  $[\epsilon, \infty)$ , and taking  $\epsilon \rightarrow 0$ , we see that the  $(-\infty, \epsilon)$  portion vanishes, giving

$$\sum_{n=1}^N \int_+ \frac{p(x_n|x_n \neq 0, \mathbf{y}; \mathbf{q}^i) \omega_k^i \mathcal{N}(x_n; \theta_k^i, \phi_k) / \Phi_c(-\theta_k^i/\sqrt{\phi_k^i})}{\zeta_n (\omega_k^i \mathcal{N}_+(x_n; \theta_k^i, \phi_k) + \sum_{\ell \neq k} \omega_\ell^i \mathcal{N}_+(x_n; \theta_\ell^i, \phi_\ell^i))} \times \left( \frac{(x_n - \theta_k^i)^2}{\phi_k} - 1 \right) = 0. \quad (101)$$

Again, this integral is difficult to compute, so we apply the approximation  $\mathcal{N}(x_n; \theta_k, \phi_k^i) \approx \mathcal{N}(x_n; \theta_k^i, \phi_k^i)$  in both the numerator and denominator. After some cancellation (as in (96)), we get the necessary condition

$$\sum_{n=1}^N \int_+ \frac{\mathcal{N}(x_n; \hat{r}_n, \mu_n^r) \omega_k^i \mathcal{N}_+(x_n; \theta_k^i, \phi_k^i)}{\zeta_n} \left( \frac{(x_n - \theta_k^i)^2}{\phi_k} - 1 \right) = 0. \quad (102)$$

To find the value of  $\phi_k$  that solves (102), we expand  $(x_n - \theta_k^i)^2 = x_n^2 - 2x_n\theta_k^i + (\theta_k^i)^2$  and apply the Gaussian-pdf multiplication rule, yielding

$$\sum_{n=1}^N \frac{\beta_{n,k}}{\Phi_c(\alpha_{n,k})} \int_+ \mathcal{N}(x_n; \gamma_{n,k}, \nu_{n,k}) \left( \frac{x_n^2 - 2x_n\theta_k^i + (\theta_k^i)^2}{\phi_k} - 1 \right) = 0. \quad (103)$$

Using similar techniques as in Appendix B-A and simplifying, we see that  $\phi_k^{i+1}$  in (57) is the value of  $\phi_k$  that solves (103).

Finally, we calculate the EM update in (55) for positive  $\omega$  under the pmf constraint  $\sum_{k=1}^L \omega_k = 1$  by solving the unconstrained optimization problem  $\max_{\omega, \xi} J(\omega, \xi)$ , where  $\xi$  is a Lagrange multiplier and

$$J(\omega, \xi) \triangleq \sum_{n=1}^N \widehat{\mathbb{E}} \{ \ln p_X(x_n; \omega, \mathbf{q}^i_{\omega}) | \mathbf{y}; \mathbf{q}^i \} - \xi \left( \sum_{\ell=1}^L \omega_\ell - 1 \right). \quad (104)$$

First, we set  $\frac{d}{d\omega_k} J(\omega, \xi) = 0$ , which yields

$$\sum_{n=1}^N \int_{x_n} \frac{p_X(x_n; \mathbf{q}^i) \mathcal{N}(x_n; \hat{r}_n, \mu_n^r)}{\zeta_n} \frac{d}{d\omega_k} \ln p_X(x_n; \omega, \mathbf{q}^i_{\omega}) = \xi. \quad (105)$$

where, for non-negative  $x_n$ ,

$$\frac{d}{d\omega_k} \ln p_X(x_n; \omega, \mathbf{q}^i_{\omega}) = \frac{\tau^i \mathcal{N}_+(x_n; \theta_k^i, \phi_k^i)}{p_X(x_n; \omega, \mathbf{q}^i_{\omega})}. \quad (106)$$

Inserting (106) into (105), we get

$$\sum_{n=1}^N \int_+ \frac{p_X(x_n; \mathbf{q}^i) \mathcal{N}(x_n; \hat{r}_n, \mu_n^r)}{\zeta_n} \frac{\tau^i \mathcal{N}_+(x_n; \theta_k^i, \phi_k^i)}{p_X(x_n; \omega, \mathbf{q}^i_{\omega})} = \xi. \quad (107)$$

As in (96) and (101), the above integral is difficult to evaluate, and so we apply the additional approximation  $\omega \approx \omega^i$ , which reduces the previous equation to

$$\xi = \sum_{n=1}^N \int_+ \frac{\tau^i \mathcal{N}_+(x_n; \theta_k^i, \phi_k^i) \mathcal{N}(x_n; \hat{r}_n, \mu_n^r)}{\zeta_n}. \quad (108)$$

We then multiply both sides by  $\omega_k^i$  for  $k = 1, \dots, L$ , and sum over  $k$ . Leveraging the fact  $1 = \sum_k \omega_k^i$ , and simplifying, we obtain the equivalent condition

$$\xi = \sum_{n=1}^N \int_+ \frac{\tau^i \sum_{k=1}^L \omega_k^i \mathcal{N}_+(x_n; \theta_k^i, \phi_k^i) \mathcal{N}(x_n; \hat{r}_n, \mu_n^r)}{\zeta_n}, \quad (109)$$

$$= \sum_{n=1}^N \frac{\tau^i}{\zeta_n} \sum_{k=1}^L \beta_{n,k} \int_+ \frac{\mathcal{N}(x_n; \gamma_{n,k}, \phi_{n,k})}{\Phi_c(\alpha_{n,k})} = \sum_{n=1}^N \pi_n. \quad (110)$$

Plugging (110) into (108) and multiplying both sides by  $\omega_k$ , the derivative-zeroing value of  $\omega_k$  is seen to be

$$\omega_k = \frac{\sum_{n=1}^N \int_+ \tau^i \omega_k \mathcal{N}_+(x_n; \theta_k^i, \phi_k^i) \mathcal{N}(x_n; \hat{r}_n, \mu_n^r) / \zeta_n}{\sum_{n=1}^N \pi_n}, \quad (111)$$

where, if we use  $\omega_k \approx \omega_k^i$  on the right of (105), then we obtain the approximate EM update  $\omega_k^{i+1}$  in (58).

## REFERENCES

- [1] J. Vila and P. Schniter, "An empirical-bayes approach to recovering linearly constrained non-negative sparse signals," in *Proc. IEEE Workshop Comp. Adv. Multi-Sensor Adaptive Process.*, (Saint Martin), Dec. 2013.
- [2] J. Bioucas-Dias, A. Plaza, N. Dobigeon, M. Parente, Q. Du, P. Gader, and J. Chanussot, "Hyperspectral unmixing overview: Geometrical, statistical, and sparse regression-based approaches," *IEEE J. Sel. Topics Appl. Earth Observ.*, vol. 5, no. 2, pp. 354–379, 2012.
- [3] H. Markowitz, *Portfolio Selection: Efficient Diversification of Investments*. New York: Wiley, 1991.
- [4] J. Brodie, I. Daubechies, C. De Mol, D. Giannone, and I. Loris, "Sparse and stable Markowitz portfolios," *Proc. Nat. Acad. Sci.*, vol. 106, no. 30, pp. 12267–12272, 2009.
- [5] B. M. Jedynek and S. Khudanpur, "Maximum likelihood set for estimating a probability mass function," *Neural Comput.*, vol. 17, pp. 1508–1530, July 2005.
- [6] A. Kyriillidis, S. Becker, V. Cevher, and C. Koch, "Sparse projections onto the simplex," *arXiv:1206.1529*, Apr. 2013.
- [7] D. L. Donoho and J. Tanner, "Sparse nonnegative solution of underdetermined linear equations by linear programming," *Proc. Nat. Acad. Sci.*, vol. 102, no. 27, pp. 9446–9451, 2005.
- [8] A. M. Bruckstein, M. Elad, and M. Zibulevsky, "On the uniqueness of nonnegative sparse solutions to underdetermined systems of equations," *IEEE Trans. Inform. Theory*, vol. 54, pp. 4813–4820, Nov. 2008.
- [9] M. A. Khajehnejad, A. Dimakis, W. Xu, and B. Hassibi, "Sparse recovery of nonnegative signals with minimal expansion," *IEEE Trans. Signal Process.*, vol. 59, pp. 198–208, Jan. 2011.
- [10] J. Romberg, "Imaging via compressive sampling," *IEEE Signal Process. Mag.*, vol. 25, pp. 14–20, Mar. 2008.
- [11] D. Chen and R. J. Plemmons, "Nonnegativity constraints in numerical analysis," in *The Birth of Numerical Analysis* (A. Bultheel and R. Cools, eds.), pp. 109–140, World Scientific Publishing Co., 2009.
- [12] D. Bertsekas, *Nonlinear Programming*. Athena Scientific, 2nd ed., 1999.
- [13] R. Giryes, M. Elad, and Y. C. Eldar, "The projectured GSURE for automatic parameter tuning in iterative shrinkage methods," *Appl. Computational Harmonic Anal.*, vol. 30, no. 2, pp. 407–422, 2011.
- [14] M. Slawski and M. Hein, "Non-negative least squares for high-dimensional linear models: consistency and sparse recovery without regularization," *arXiv:1205.0953*, 2012.
- [15] R. Garg and R. Khandekar, "Gradient descent with sparsification: an iterative algorithm for sparse recovery with restricted isometry property," in *Proc. Int. Conf. Mach. Learning*, (New York), pp. 337–344, 2009.
- [16] S. Rangan, "Generalized approximate message passing for estimation with random linear mixing," in *Proc. IEEE Int. Symp. Inform. Thy.*, (Saint Petersburg, Russia), pp. 2168–2172, Aug. 2011. (Full version at *arXiv:1010.5141*).
- [17] S. Rangan, P. Schniter, E. Riegler, A. Fletcher, and V. Cevher, "Fixed points of generalized approximate message passing with arbitrary matrices," in *Proc. IEEE Int. Symp. Inform. Thy.*, (Istanbul, Turkey), July 2013. (Full version at *arXiv:1301.6295*).
- [18] A. Dempster, N. M. Laird, and D. B. Rubin, "Maximum-likelihood from incomplete data via the EM algorithm," *J. Roy. Statist. Soc.*, vol. 39, pp. 1–17, 1977.
- [19] R. Tibshirani, "Regression shrinkage and selection via the lasso," *J. Roy. Statist. Soc. B*, vol. 58, no. 1, pp. 267–288, 1996.
- [20] S. S. Chen, D. L. Donoho, and M. A. Saunders, "Atomic decomposition by basis pursuit," *SIAM J. Scientific Comput.*, vol. 20, no. 1, pp. 33–61, 1998.
- [21] S. Becker, E. Candès, and M. M. Grant, "Templates for convex cone problems with applications to sparse signal recovery," *Math. Program. Comput.*, vol. 3, no. 3, pp. 165–218, 2011.
- [22] P. Bloomfield and W. L. Steiger, *Least Absolute Deviations: Theory, Applications, and Algorithms*. Boston: Birkhäuser, 1984.
- [23] J. P. Vila and P. Schniter, "Expectation-maximization Gaussian-mixture approximate message passing," *IEEE Trans. Signal Process.*, vol. 61, pp. 4658–4672, Oct. 2013.
- [24] A. Javanmard and A. Montanari, "State evolution for general approximate message passing algorithms, with applications to spatial coupling," *arXiv:1211.5164*, Nov. 2012.
- [25] U. S. Kamilov, S. Rangan, A. K. Fletcher, and M. Unser, "Approximate message passing with consistent parameter estimation and applications to sparse learning," in *Proc. Neural Inform. Process. Syst. Conf.*, (Lake Tahoe, NV), pp. 2447–2455, Dec. 2012. (Full version at *arXiv:1207.3859*).
- [26] B. Efron, *Large-Scale Inference: Empirical Bayes Methods for Estimation, Testing, and Prediction*. New York: Cambridge University Press, 2010.
- [27] D. L. Donoho, A. Maleki, and A. Montanari, "Message passing algorithms for compressed sensing," *Proc. Nat. Acad. Sci.*, vol. 106, pp. 18914–18919, Nov. 2009.
- [28] D. L. Donoho, A. Maleki, and A. Montanari, "Message passing algorithms for compressed sensing: II. Analysis and validation," in *Proc. Inform. Theory Workshop*, (Cairo, Egypt), pp. 1–5, Jan. 2010.
- [29] H. Monajemi, S. Jafarpour, M. Gavish, Stat 330/CME 362 Collaboration, and D. L. Donoho, "Deterministic matrices matching the compressed sensing phase transitions of Gaussian random matrices," *Proc. Nat. Acad. Sci.*, vol. 110, pp. 1181–1186, Jan. 2013.
- [30] C. F. J. Wu, "On the convergence properties of the EM algorithm," *Ann. Statist.*, vol. 11, no. 1, pp. 95–103, 1983.
- [31] R. Neal and G. Hinton, "A view of the EM algorithm that justifies incremental, sparse, and other variants," in *Learning in Graphical Models* (M. I. Jordan, ed.), pp. 355–368, MIT Press, 1999.
- [32] P. Stoica and Y. Selén, "Model-order selection: A review of information criterion rules," *IEEE Signal Process. Mag.*, vol. 21, pp. 36–47, July 2004.
- [33] C. M. Bishop, *Pattern Recognition and Machine Learning*. New York: Springer, 2007.
- [34] E. van den Berg and M. P. Friedlander, "Probing the Pareto frontier for basis pursuit solutions," *SIAM J. Scientific Comput.*, vol. 31, no. 2, pp. 890–912, 2008.
- [35] V. DeMiguel, L. Garlappi, and R. Uppal, "Optimal versus naive diversification: How inefficient is the 1-n portfolio strategy?," *Rev. of Financ. Stud.*, vol. 22, pp. 1915–1953, May 2009.
- [36] A. Giannandrea, N. Raqueno, D. W. Messinger, J. Faulring, J. P. Kerekes, J. van Aardt, K. Canham, S. Hagstrom, E. Ontiveros, A. Gerace, J. Kaufman, K. M. Vongsy, H. Griffith, B. D. Bartlett, E. Ientilucci, J. Meola, L. Scarff, and B. Daniels, "The SHARE 2012 data collection campaign," *Proc. SPIE*, vol. 8743, p. 15, 2013.
- [37] K. Canham, D. Goldberg, J. Kerekes, N. Raqueno, and D. Messinger, "SHARE 2012: Large edge targets for hyperspectral imaging applications," *Proc. SPIE*, vol. 8743, no. 87430G, p. 9, 2013.
- [38] J. Nascimento and J. Bioucas Dias, "Vertex component analysis: a fast algorithm to unmix hyperspectral data," *IEEE Trans. Geosci. Remote Sens.*, vol. 43, no. 4, pp. 898–910, 2005.
- [39] D. Heinz and C.-I. Chang, "Fully constrained least squares linear spectral mixture analysis method for material quantification in hyperspectral imagery," *IEEE Trans. Geosci. Remote Sens.*, vol. 39, no. 3, pp. 529–545, 2001.
- [40] M. E. Winter, "N-FINDR: an algorithm for fast autonomous spectral end-member determination in hyperspectral data," *Proc. SPIE*, pp. 266–275, 1999.
- [41] N. Gillis and S. A. Vavasis, "Fast and robust recursive algorithms for separable nonnegative matrix factorization," *arXiv:1208.1237v2*, 2012.
- [42] J. Parker, P. Schniter, and V. Cevher, "Bilinear generalized approximate message passing," 2013.
- [43] P. Schniter, "Turbo reconstruction of structured sparse signals," in *Proc. Conf. Inform. Science & Syst.*, (Princeton, NJ), pp. 1–6, Mar. 2010.
- [44] J. Vila, P. Schniter, and J. Meola, "Hyperspectral image unmixing via bilinear generalized approximate message passing," *Proc. SPIE*, vol. 8743, no. 87430Y, p. 9, 2013.
- [45] N. L. Johnson, S. Kotz, and N. Balakrishnan, *Continuous Univariate Distributions*, vol. 2. New York: Wiley & Sons, 1995.